

# Impact of quark flavor violating SUSY on $h(125)$ decays at future lepton colliders

Helmut Eberl<sup>1</sup>, Keisho Hidaka<sup>2</sup>, Elena Ginina<sup>1</sup>

<sup>1</sup> *Institut für Hochenergiephysik der Österreichischen Akademie der Wissenschaften, A-1050 Vienna, Austria*

<sup>2</sup> *Department of Physics, Tokyo Gakugei University, Koganei, Tokyo 184-8501, Japan*

## Abstract

We study the CP-even neutral Higgs boson decays  $h^0 \rightarrow c\bar{c}, b\bar{b}, b\bar{s}, \gamma\gamma, gg$  in the Minimal Supersymmetric Standard Model (MSSM) with general quark flavor violation (QFV) due to squark generation mixings, identifying the  $h^0$  as the Higgs boson with a mass of 125 GeV. We compute the widths of the  $h^0$  decays to  $c\bar{c}, b\bar{b}, b\bar{s}$  at full one-loop level. For the  $h^0$  decays to  $\gamma\gamma$  and  $gg$  we compute the widths at NLO QCD level. *For the first time*, we perform a systematic MSSM parameter scan for these widths respecting all the relevant theoretical and experimental constraints, such as those from B-meson data, and the 125 GeV Higgs boson data from recent LHC experiments, as well as the limits on Supersymmetric (SUSY) particle (sparticle) masses from the LHC experiments. We also take into account the expected sparticle mass limits from the future HL-LHC experiment in our analysis. *In strong contrast to* the usual studies in the MSSM with Minimal Flavor Violation (MFV), we find that the deviations of these MSSM decay widths from the Standard Model (SM) values can be quite sizable and that there are significant correlations among these deviations. All of these sizable deviations in the  $h^0$  decays are mainly due to large charm-stop mixing and large strange-sbottom mixing. Such sizable deviations from the SM can be observed at high signal significance in future lepton colliders such as ILC, CLIC, CEPC, FCC-ee and muon collider *even after* the failure of SUSY particle discovery at the HL-LHC. In case the deviation pattern shown here is really observed at the lepton colliders, then it would strongly suggest the discovery of QFV SUSY (the MSSM with general QFV).

# 1 Introduction

What is the Standard Model (SM)-like Higgs boson with mass of 125 GeV discovered at LHC [1, 2]? It can be the Higgs boson of the SM. It can be a Higgs boson of a New Physics (NP) theory beyond the SM. This is one of the most important issues in the field of present particle physics. The detailed study of the properties (such as mass and couplings) of the SM-like Higgs boson could shed light on this issue and the way to the NP theory [3]. Here we study a possibility that the discovered SM-like Higgs boson is the lighter CP even neutral Higgs boson  $h^0$  of the Minimal Supersymmetric Standard Model (MSSM), focusing on the decays  $h^0 \rightarrow c\bar{c}, b\bar{b}, b\bar{s}, \gamma\gamma, gg$ , where  $c, b, s, \gamma$  and  $g$  are  $c$ -,  $b$ -,  $s$ -quarks, photon and gluon, respectively. In order to investigate such a possibility we compute the widths of these decays in the MSSM with general quark-flavor violation (QFV) due to squark generation mixing according to our previous works [4–6] and study the deviations of the MSSM widths from the SM widths.

The deviations of the SM-like Higgs boson decay widths from their SM values are usually estimated to be rather small (typically several % level or less) in the MSSM with Minimal Flavor Violation (MFV) where the only source of quark-flavor violation is the Cabibbo-Kobayashi-Maskawa (CKM) quark-mixing matrix [7–12].

In the present article, however, we show that the situation changes drastically yielding significant enhancement of the deviations in the widths once we switch-on the general QFV in the MSSM, by performing a systematic MSSM parameter scan respecting all the relevant theoretical and experimental constraints <sup>1</sup>.

In [14–19] it was shown that the general QFV in the MSSM can also enhance QFV decays  $h^0 \rightarrow b\bar{s}$  and  $h^0 \rightarrow \bar{b}s$ . These analyses are rather old. In the present paper we update them, especially by taking into account the expected mass limits for the superpartner particles and the heavier MSSM Higgs bosons  $H^0, A^0, H^\pm$  from the future HL-LHC experiment.

On the experimental side, the widths of these decays,  $h^0 \rightarrow c\bar{c}, b\bar{b}, \gamma\gamma, gg$  (or corresponding effective couplings) can be measured precisely and *model-independently* at future lepton colliders, such as ILC, CLIC, CEPC, FCC-ee and muon-collider (MuC) [20, 21] <sup>2</sup>. This enables us to clarify the possibility that the discovered SM-like Higgs boson is the lighter CP even neutral Higgs boson  $h^0$  of the MSSM.

In Section 2 we introduce the supersymmetric (SUSY) QFV parameters originating from the squark mass matrices. Details of our parameter scan are given in Section 3. In Section 4 we study the deviations of the MSSM widths from the SM widths for the decays  $h^0 \rightarrow c\bar{c}, b\bar{b}, b\bar{s}, \gamma\gamma, gg$  and analyze their behavior in the MSSM with general QFV. The

---

<sup>1</sup>The decay  $h^0 \rightarrow c\bar{c}$  was not studied in [7–12]. The decays  $h^0 \rightarrow c\bar{c}, \gamma\gamma, gg$  in the MSSM with QFV were studied in [13]. However, the important QFV parameters  $M_{Q23}^2, M_{U23}^2$ , and  $M_{D23}^2$  (which are defined in Section 2) were neglected and the systematic MSSM parameter scan respecting all the relevant theoretical and experimental constraints was not performed in [13].

<sup>2</sup>The effective couplings of  $g(h^0 b\bar{b}), g(h^0 \gamma\gamma)$  and  $g(h^0 gg)$  can be measured rather precisely but *model-dependently* by a global fit at HL-LHC [20–22]. Moreover, it is difficult to measure the coupling  $g(h^0 c\bar{c})$  at LHC and HL-LHC due to the difficulty of the  $c$ -tagging and the huge hadronic QCD background [22].

summary and conclusion are in Section 5. All relevant constraints are listed in Appendix A and the expected errors in the deviation measurements at future lepton colliders are listed in Appendix B. ILC sensitivity to the branching ratio  $B(h^0 \rightarrow bs)$  is discussed in Appendix C, and consistency of the MSSM predictions for coupling modifiers with the LHC data is discussed in Appendix D.

## 2 Squark mass matrices in the MSSM with general QFV

In the super-CKM basis of  $\tilde{q}_{0\gamma} = (\tilde{q}_{1L}, \tilde{q}_{2L}, \tilde{q}_{3L}, \tilde{q}_{1R}, \tilde{q}_{2R}, \tilde{q}_{3R})$ ,  $\gamma = 1, \dots, 6$ , with  $(q_1, q_2, q_3) = (u, c, t), (d, s, b)$ , the up-type and down-type squark mass squared matrices  $\mathcal{M}_{\tilde{q}}^2$ ,  $\tilde{q} = \tilde{u}, \tilde{d}$ , at the SUSY scale have the following most general  $3 \times 3$  block form [23]:

$$\mathcal{M}_{\tilde{q}}^2 = \begin{pmatrix} \mathcal{M}_{\tilde{q},LL}^2 & \mathcal{M}_{\tilde{q},LR}^2 \\ \mathcal{M}_{\tilde{q},RL}^2 & \mathcal{M}_{\tilde{q},RR}^2 \end{pmatrix}, \quad \tilde{q} = \tilde{u}, \tilde{d}. \quad (1)$$

Non-zero off-diagonal terms of the  $3 \times 3$  blocks  $\mathcal{M}_{\tilde{q},LL}^2$ ,  $\mathcal{M}_{\tilde{q},RR}^2$ ,  $\mathcal{M}_{\tilde{q},LR}^2$  and  $\mathcal{M}_{\tilde{q},RL}^2$  explicitly violate quark-flavor in the squark sector of the MSSM. The left-left and right-right blocks in Eq. (1) are given by

$$\begin{aligned} \mathcal{M}_{\tilde{u}(\tilde{d}),LL}^2 &= M_{Q_{u(d)}}^2 + D_{\tilde{u}(\tilde{d}),LL} \mathbf{1} + \hat{m}_{u(d)}^2, \\ \mathcal{M}_{\tilde{u}(\tilde{d}),RR}^2 &= M_{U(D)}^2 + D_{\tilde{u}(\tilde{d}),RR} \mathbf{1} + \hat{m}_{u(d)}^2, \end{aligned} \quad (2)$$

where  $M_{Q_u}^2 = V_{\text{CKM}} M_Q^2 V_{\text{CKM}}^\dagger$ ,  $M_{Q_d}^2 \equiv M_Q^2$ ,  $M_{Q,U,D}^2$  are the hermitian soft SUSY-breaking mass squared matrices of the squarks,  $D_{\tilde{u}(\tilde{d}),LL}$ ,  $D_{\tilde{u}(\tilde{d}),RR}$  are the  $D$ -terms, and  $\hat{m}_{u(d)}$  are the diagonal mass matrices of the up(down)-type quarks.  $M_{Q_u}^2$  is related with  $M_{Q_d}^2$  by the CKM matrix  $V_{\text{CKM}}$  due to the  $SU(2)_L$  symmetry. The left-right and right-left blocks of Eq. (1) are given by

$$\mathcal{M}_{\tilde{u}(\tilde{d}),RL}^2 = \mathcal{M}_{\tilde{u}(\tilde{d}),LR}^{2\dagger} = \frac{v_2(v_1)}{\sqrt{2}} T_{U(D)} - \mu^* \hat{m}_{u(d)} \cot \beta (\tan \beta), \quad (3)$$

where  $T_{U,D}$  are the soft SUSY-breaking trilinear coupling matrices of the up-type and down-type squarks entering the Lagrangian  $\mathcal{L}_{\text{int}} \supset -(T_{U\alpha\beta} \tilde{u}_{\alpha R}^\dagger \tilde{u}_{\beta L} H_2^0 + T_{D\alpha\beta} \tilde{d}_{\alpha R}^\dagger \tilde{d}_{\beta L} H_1^0)$ ,  $\mu$  is the higgsino mass parameter, and  $\tan \beta = v_2/v_1$  with  $v_{1,2} = \sqrt{2} \langle H_{1,2}^0 \rangle$ . The squark mass squared matrices are diagonalized by the  $6 \times 6$  unitary matrices  $U^{\tilde{q}}$ ,  $\tilde{q} = \tilde{u}, \tilde{d}$ , such that

$$U^{\tilde{q}} \mathcal{M}_{\tilde{q}}^2 (U^{\tilde{q}})^\dagger = \text{diag}(m_{\tilde{q}_1}^2, \dots, m_{\tilde{q}_6}^2), \quad (4)$$

with  $m_{\tilde{q}_1} < \dots < m_{\tilde{q}_6}$ . The physical mass eigenstates  $\tilde{q}_i, i = 1, \dots, 6$  are given by  $\tilde{q}_i = U_{i\alpha}^{\tilde{q}} \tilde{q}_{0\alpha}$ .

In this paper we focus on the  $\tilde{c}_L - \tilde{t}_L$ ,  $\tilde{c}_R - \tilde{t}_R$ ,  $\tilde{c}_R - \tilde{t}_L$ ,  $\tilde{c}_L - \tilde{t}_R$ ,  $\tilde{s}_L - \tilde{b}_L$ ,  $\tilde{s}_R - \tilde{b}_R$ ,  $\tilde{s}_R - \tilde{b}_L$ , and  $\tilde{s}_L - \tilde{b}_R$  mixing which is described by the QFV parameters  $M_{Q_{u23}}^2 \simeq M_{Q_{23}}^2$ ,

$M_{U23}^2$ ,  $T_{U23}$ ,  $T_{U32}$ ,  $M_{Q23}^2$ ,  $M_{D23}^2$ ,  $T_{D23}$  and  $T_{D32}$ , respectively. We will also often refer to the quark-flavor conserving (QFC) parameters  $T_{U33}$  and  $T_{D33}$  which induce the  $\tilde{t}_L - \tilde{t}_R$  and  $\tilde{b}_L - \tilde{b}_R$  mixing, respectively, and play an important role in this study.

The slepton parameters are defined analogously to the squark ones. In our analysis we assume that there is no SUSY lepton-flavor violation. We also assume that R-parity is conserved and that the lightest neutralino  $\tilde{\chi}_1^0$  is the lightest SUSY particle (LSP). All the parameters in this study are assumed to be real, except the CKM matrix  $V_{CKM}$ .

### 3 Parameter scan

In our MSSM parameter scan we take into account all the relevant constraints, i. e., theoretical constraints from vacuum stability conditions and experimental constraints, such as those from  $K$ - and  $B$ -meson data, electroweak precision data, and the  $H^0$  mass and coupling data from recent LHC experiments, as well as the SUSY particle (sparticle) mass limits from current LHC experiments (see Appendix A). Here  $H^0$  is the discovered SM-like Higgs boson which we identify as the lightest  $CP$  even neutral Higgs boson  $h^0$  in the MSSM. Concerning squark generation mixings, we only consider the mixing between the second and third generation of squarks. The mixing between the first and the second generation squarks is strongly constrained by the  $K$ - and  $D$ -meson data [24, 25]. The experimental constraints on the mixing of the first and third generation squarks are not so strong [26], but we do not consider this mixing since its effect is essentially similar to that of the mixing of the second and third generation squarks. We generate the input parameter points by using random numbers in the ranges shown in Table 1, where some parameters are fixed as given in the last box. All input parameters are  $\overline{\text{DR}}$  parameters defined at scale  $Q = 1$  TeV, except  $m_{A^0}(\text{pole})$  which is the pole mass of the  $CP$  odd Higgs boson  $A^0$ . The parameters that are not shown explicitly are taken to be zero. The entire scan range lies in the decoupling Higgs limit, i. e., in the scenarios with large  $\tan\beta \geq 10$  and large  $m_{A^0} \geq 1350$  GeV (see Table 1), respecting the fact that the discovered Higgs boson is SM-like. It is well known that the lightest MSSM Higgs boson  $h^0$  is SM-like (including its couplings) in this limit. We do not assume the GUT relation for the gaugino masses  $M_1$ ,  $M_2$ ,  $M_3$ . The masses and mixing matrices of the SUSY particles and the Higgs bosons are renormalized basically at one-loop level by using the public code `SPheno-v3.3.8` [27, 28]<sup>3</sup> based on the technique given in [30]. From 377180 input points generated in the scan 3208 points survived all constraints. These are 0.85% of the generated points. We show these survival points in all scatter plots in this article.

---

<sup>3</sup>This version SPheno-v3.3.8 implements full flavor (generation) mixings in the sfermion (squarks and sleptons) sector as described in Section 2 and calculates the masses and mixings of the SUSY particles and the MSSM Higgs bosons  $h^0$ ,  $H^0$ ,  $A^0$ ,  $H^\pm$  taking into accounts the full flavor mixings in the sfermion sector [29].

Table 1: Scanned ranges and fixed values of the MSSM parameters (in units of GeV or GeV<sup>2</sup>, except for  $\tan\beta$ ). The parameters that are not shown explicitly are taken to be zero.  $M_{1,2,3}$  are the U(1), SU(2), SU(3) gaugino mass parameters.

$\tan\beta$	$M_1$	$M_2$	$M_3$	$\mu$	$m_{A^0}(pole)$
$10 \div 80$	$100 \div 2500$	$100 \div 2500$	$2500 \div 5000$	$100 \div 2500$	$1350 \div 6000$
$M_{Q22}^2$	$M_{Q33}^2$	$ M_{Q23}^2 $	$M_{U22}^2$	$M_{U33}^2$	$ M_{U23}^2 $
$2500^2 \div 4000^2$	$2500^2 \div 4000^2$	$< 1000^2$	$1000^2 \div 4000^2$	$600^2 \div 3000^2$	$< 2000^2$
$M_{D22}^2$	$M_{D33}^2$	$ M_{D23}^2 $	$ T_{U23} $	$ T_{U32} $	$ T_{U33} $
$2500^2 \div 4000^2$	$1000^2 \div 3000^2$	$< 2000^2$	$< 4000$	$< 4000$	$< 5000$
$ T_{D23} $	$ T_{D32} $	$ T_{D33} $	$ T_{E33} $		
$< 3000$	$< 3000$	$< 4000$	$< 500$		

$M_{Q11}^2$	$M_{U11}^2$	$M_{D11}^2$	$M_{L11}^2$	$M_{L22}^2$	$M_{L33}^2$	$M_{E11}^2$	$M_{E22}^2$	$M_{E33}^2$
$4500^2$	$4500^2$	$4500^2$	$1500^2$	$1500^2$	$1500^2$	$1500^2$	$1500^2$	$1500^2$

## 4 125 GeV Higgs boson decays in the MSSM with general QFV

We compute the decay widths  $\Gamma(h^0 \rightarrow c\bar{c})$ ,  $\Gamma(h^0 \rightarrow b\bar{b})$  and  $\Gamma(h^0 \rightarrow b\bar{s}/\bar{b}s)$  at full 1-loop level in the  $\overline{DR}$  renormalization scheme in the MSSM with general QFV [4, 5] and study the deviation of the MSSM predictions from the SM ones. We also compute the decay widths  $\Gamma(h^0 \rightarrow gg)$  and  $\Gamma(h^0 \rightarrow \gamma\gamma)$  at the next-to-leading order (NLO) QCD level in the  $\overline{DR}$  renormalization scheme in the MSSM with general QFV [6] and study the deviation of the MSSM widths from the SM ones, where  $g$  is a gluon and  $\gamma$  is a photon. As the  $h^0$  decays to  $gg$  and  $\gamma\gamma$  are loop-induced decays, these decays are sensitive to New Physics.

Here, we remark the differences between our previous works [4–6] and the present work: In the present work, we update the constraints on the MSSM parameters significantly including the expected sparticle mass limits from the future HL-LHC experiments, and study also the branching ratio of the explicitly QFV decay  $B(h^0 \rightarrow b\bar{s}/\bar{b}s)$  and the correlations among the deviations of the MSSM widths of the various decay modes from the corresponding SM ones.

## 4.1 Expectations

We find that large squark trilinear couplings  $T_{U23,32,33}$ ,  $T_{D23,32,33}$ , large  $M_{Q23}^2$ ,  $M_{U23}^2$ ,  $M_{D23}^2$ , large bottom Yukawa coupling  $Y_b$  for large  $\tan\beta$ , and large top Yukawa coupling  $Y_t$  can lead to large MSSM 1-loop contributions to these decay widths, resulting in sizable deviation of the MSSM widths from the SM values. This is mainly due to the following reasons:

The lighter up-type squarks  $\tilde{u}_{1,2,3}$  are strong  $\tilde{c}_{L,R} - \tilde{t}_{L,R}$  mixtures for large  $M_{Q23}^2$ ,  $M_{U23}^2$ ,  $T_{U23,32,33}$ . The lighter down-type squarks  $\tilde{d}_{1,2,3}$  are strong  $\tilde{s}_{L,R} - \tilde{b}_{L,R}$  mixtures for large  $M_{Q23}^2$ ,  $M_{D23}^2$ ,  $T_{D23,32,33}$ . Here note that  $|T_{U23,32,33}|$  the size of which are controlled by  $Y_t$  due to the vacuum stability conditions can be large because of large  $Y_t$  and that  $|T_{D23,32,33}|$  the size of which are controlled by  $Y_b$  due to the vacuum stability conditions can be large thanks to large  $Y_b$  for large  $\tan\beta$  (see Eqs. (11 - 14) in Appendix A). In the following we assume these setups.

### 4.1.1 Expectations for fermionic decays

The main MSSM 1-loop corrections to  $\Gamma(h^0 \rightarrow c\bar{c})$  stem from the lighter up-type squarks ( $\tilde{u}_{1,2,3}$ ) - gluino ( $\tilde{g}$ ) loops at the decay vertex which have  $h^0 - \tilde{u}_i - \tilde{u}_j$  couplings containing  $H_2^0 - \tilde{c}_R - \tilde{t}_L$ ,  $H_2^0 - \tilde{c}_L - \tilde{t}_R$ ,  $H_2^0 - \tilde{t}_L - \tilde{t}_R$  couplings, i. e.,  $T_{U23,32,33}$  (see Fig. 1(a)). Note that  $h^0$  is a mixture of  $Re(H_1^0)$  (which couples to the down-type squarks  $\tilde{d}_i$ ) and  $Re(H_2^0)$  (which couples to the up-type squarks  $\tilde{u}_i$ ), i. e.,  $h^0 = -\sin\alpha(\sqrt{2}Re(H_1^0) - v_1) + \cos\alpha(\sqrt{2}Re(H_2^0) - v_2)$  and that  $h^0$  is dominated by  $Re(H_2^0)$  component in our decoupling Higgs scenario with large  $m_{A^0}$  ( $> 1350$  GeV) and large  $\tan\beta$  ( $> 10$ ) (see Table 1). Hence, the large  $Re(H_2^0)$  component of  $h^0$  and the large trilinear couplings  $T_{U23,32,33}$  can enhance the  $h^0 - \tilde{u}_i - \tilde{u}_j$  couplings, which together with the large QCD couplings involved can result in a strong enhancement of the  $\tilde{u}_i$ - $\tilde{g}$  loop corrections to  $\Gamma(h^0 \rightarrow c\bar{c})$ , leading to a large deviation of the MSSM width  $\Gamma(h^0 \rightarrow c\bar{c})$  from its SM value.

Here note that  $\tilde{u}_i$  - neutralino ( $\tilde{\chi}_i^0$ ) loops and  $\tilde{d}_i$  - chargino ( $\tilde{\chi}_{1,2}^\pm$ ) loops at the decay vertex are not so important by the following reason with  $\tilde{\chi}_i^0$  and  $\tilde{\chi}_{1,2}^\pm$  being mixtures of photino  $\tilde{\gamma}$ , zino  $\tilde{Z}$ , and neutral higgsinos  $\tilde{H}_{1,2}^0$  and mixtures of charged wino  $\tilde{W}^\pm$  and charged higgsino  $\tilde{H}^\pm$ , respectively: (i) The former loops where  $h^0$  directly couples to  $\tilde{u}_i - \tilde{u}_j$  are suppressed by the relatively small electroweak-Yukawa couplings of the neutralino to  $c$  and  $\tilde{u}_i$  compared with the QCD couplings of gluino to  $c$  and  $\tilde{u}_i$  in the  $\tilde{u}_i$ - $\tilde{g}$  loops. (ii) The former loops where  $h^0$  directly couples to the neutralino are also suppressed by the relatively small couplings of the neutralino and cannot be enhanced by the large trilinear couplings  $T_{U23,32,33}$ . (iii) The latter loops where  $h^0$  directly couples to  $\tilde{d}_i - \tilde{d}_j$  are suppressed by the small  $Re(H_1^0)$  component of  $h^0$  though they can be enhanced by the large trilinear couplings  $T_{D23,32,33}$ . They are further suppressed by the relatively small electroweak-Yukawa couplings of the chargino to  $c$  and  $\tilde{d}_i$  compared with the QCD couplings. (iv) The latter loops where  $h^0$  directly couples to the chargino are also suppressed by the relatively small electroweak-Yukawa couplings of the chargino to  $c$  and  $\tilde{d}_i$  and cannot be enhanced by the large trilinear couplings  $T_{D23,32,33}$ .

The main MSSM 1-loop corrections to  $\Gamma(h^0 \rightarrow b\bar{b})$  and  $\Gamma(h^0 \rightarrow b\bar{s}/\bar{b}s)$  stem from (i)  $\tilde{u}_{1,2,3}$  - chargino ( $\tilde{\chi}_{1,2}^\pm$ ) loops at the decay vertex which have  $h^0 - \tilde{u}_i - \tilde{u}_j$  couplings to be enhanced by large  $T_{U23,32,33}$  (see Fig. 1(b))<sup>4</sup> and (ii)  $\tilde{d}_{1,2,3}$  -  $\tilde{g}$  loops at the decay vertex which have  $h^0 - \tilde{d}_i - \tilde{d}_j$  couplings containing  $H_1^0 - \tilde{s}_R - \tilde{b}_L$ ,  $H_1^0 - \tilde{s}_L - \tilde{b}_R$ ,  $H_1^0 - \tilde{b}_L - \tilde{b}_R$  couplings, i. e.,  $T_{D23,32,33}$  (see Fig. 1(c))<sup>5</sup>. Hence large trilinear couplings  $T_{U23,32,33}$  and  $T_{D23,32,33}$  can enhance the MSSM 1-loop corrections to  $\Gamma(h^0 \rightarrow b\bar{b})$  and  $\Gamma(h^0 \rightarrow b\bar{s}/\bar{b}s)$  due to the  $\tilde{u}_i - \tilde{\chi}_{1,2}^\pm$  and  $\tilde{d}_i - \tilde{g}$  loops, leading to large deviation of the MSSM widths  $\Gamma(h^0 \rightarrow b\bar{b})$  and  $\Gamma(h^0 \rightarrow b\bar{s}/\bar{b}s)$  from their SM values.

Note that the wave function corrections for the external  $h^0$  in the decays  $h^0 \rightarrow c\bar{c}/b\bar{b}$  which have the  $h^0 - \tilde{u}_i - \tilde{u}_j$  and  $h^0 - \tilde{d}_i - \tilde{d}_j$  couplings (for  $\tilde{u}_i$  and  $\tilde{d}_i$  loops, respectively) can also be enhanced by the large trilinear couplings  $T_{U23,32,33}$  and  $T_{D23,32,33}$ , resulting in a further enhancement of the MSSM 1-loop corrections to the widths  $\Gamma(h^0 \rightarrow c\bar{c}/b\bar{b})$ .

Here we remark that the MSSM one-loop corrections to the decay amplitude for  $h^0 \rightarrow c\bar{c}$  are expected to be significantly larger than those for  $h^0 \rightarrow b\bar{b}$  due to the following reasons:

- (i) The main MSSM 1-loop corrections to  $h^0 \rightarrow c\bar{c}$  stem from  $\tilde{u}_i - \tilde{g}$  loops (Fig. 1(a)). The main MSSM 1-loop corrections to  $h^0 \rightarrow b\bar{b}$  stem from  $\tilde{u}_i - \tilde{\chi}_j^\pm$  loops (Fig. 1(b)) and  $\tilde{d}_i - \tilde{g}$  loops (Fig. 1(c)).
- (ii) The  $\tilde{u}_i - \tilde{\chi}_j^\pm$  loops of Fig. 1(b) are suppressed by the relatively small electroweak-Yukawa couplings of  $\tilde{\chi}_j^\pm$  compared with the  $\tilde{u}_i - \tilde{g}$  loops of Fig. 1(a) having the large QCD couplings of  $\tilde{g}$ .
- (iii) The  $\tilde{d}_i - \tilde{g}$  loops of Fig. 1(c) are suppressed by the relatively small  $h^0 - \tilde{d}_i - \tilde{d}_j$  couplings due to the small  $Re(H_1^0)$  component of  $h^0$  compared with the  $\tilde{u}_i - \tilde{g}$  loops of Fig. 1(a).
- (iv) Hence the MSSM one-loop corrections to the decay amplitude for  $h^0 \rightarrow c\bar{c}$  (Fig. 1(a)) are expected to be significantly larger than those for  $h^0 \rightarrow b\bar{b}$  (Fig. 1(b) + Fig. 1(c)).

On the other hand, the SM width  $\Gamma(h^0 \rightarrow c\bar{c})_{SM}$  is much smaller than  $\Gamma(h^0 \rightarrow b\bar{b})_{SM}$  mainly due to the much smaller charm Yukawa coupling than the bottom Yukawa one, which together with the item (iv) results in *much larger* relative deviation of the MSSM width from the SM width for the decay  $h^0 \rightarrow c\bar{c}$  than that for  $h^0 \rightarrow b\bar{b}$  (see Eq.(5)) *in strong contrast to usual expectations*. We will see this tendency explicitly in the plots shown below (e.g. see Fig. 3).

---

<sup>4</sup>Note that the  $\tilde{u}_{1,2,3} - \tilde{\chi}_{1,2}^\pm$  loops where  $h^0$  couples directly to  $\tilde{\chi}_{1,2}^\pm$  cannot be enhanced by the large  $T_{U23,32,33}$  and hence they are not so important.

<sup>5</sup>Here note that the  $h^0 - \tilde{d}_i - \tilde{d}_j$  couplings are suppressed by the small  $Re(H_1^0)$  component of  $h^0$ , but can be enhanced by large  $T_{D23,32,33}$ . Note also that  $\tilde{d}_{1,2,3} - \tilde{\chi}_i^0$  loops at the decay vertex are not so important compared with  $\tilde{d}_{1,2,3} - \tilde{g}$  loops at the vertex by a reason similar to the reason why the  $\tilde{u}_i - \tilde{\chi}_i^0$  loop corrections to  $\Gamma(h^0 \rightarrow c\bar{c})$  are suppressed compared with the  $\tilde{u}_i - \tilde{g}$  loop corrections.

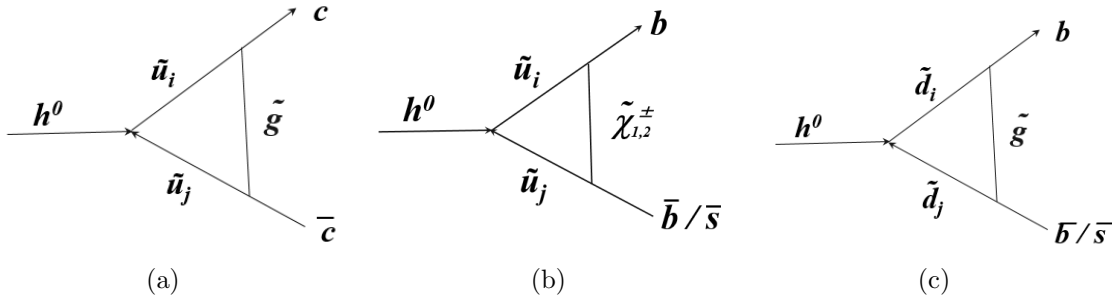


Figure 1: (a) The  $\tilde{u}_i$ - $\tilde{g}$  loop corrections to  $\Gamma(h^0 \rightarrow c\bar{c})$ , (b) the  $\tilde{u}_i$ - $\tilde{\chi}_{1,2}^\pm$  loop and (c) the  $\tilde{d}_i$ - $\tilde{g}$  loop corrections to  $\Gamma(h^0 \rightarrow b\bar{b}/\bar{s})$ .

#### 4.1.2 Expectations for bosonic decays

Similar arguments hold for the loop-induced decays  $h^0 \rightarrow gg, \gamma\gamma$ . The main SM 1-loop contribution to  $\Gamma(h^0 \rightarrow gg)$  stems from the top-quark loop. The bottom-quark loop contribution to this width is much suppressed by the small  $Re(H_1^0)$  component of  $h^0$  in our decoupling Higgs scenario. The main MSSM 1-loop contributions to  $\Gamma(h^0 \rightarrow gg)$  stem from the lighter up-type squark ( $\tilde{u}_{1,2,3}$ ) loops which have  $h^0 - \tilde{u}_i - \tilde{u}_i$  couplings (see Fig. 2(a)). The large trilinear couplings  $T_{U23,32,33}$  can enhance the  $h^0 - \tilde{u}_i - \tilde{u}_i$  couplings and hence the  $\tilde{u}_i$  loops, resulting in sizable deviation of the MSSM width  $\Gamma(h^0 \rightarrow gg)$  from its SM value. The lighter down-type squark ( $\tilde{d}_{1,2,3}$ ) loop contributions to this width are suppressed by the small  $Re(H_1^0)$  component of  $h^0$ .

The main SM 1-loop contributions to  $\Gamma(h^0 \rightarrow \gamma\gamma)$  stem from  $W^+$  boson and top-quark loops. The bottom-quark and tau-lepton loop contributions to this width are suppressed by the small  $Re(H_1^0)$  component of  $h^0$ . The main MSSM 1-loop contributions to  $\Gamma(h^0 \rightarrow \gamma\gamma)$  stem from the lighter up-type squark ( $\tilde{u}_{1,2,3}$ ) loops which have  $h^0 - \tilde{u}_i - \tilde{u}_i$  couplings (see Fig. 2(b)). The large trilinear couplings  $T_{U23,32,33}$  can enhance the  $h^0 - \tilde{u}_i - \tilde{u}_i$  couplings and hence the  $\tilde{u}_i$  loops, leading to sizable deviation of the MSSM width  $\Gamma(h^0 \rightarrow \gamma\gamma)$  from its SM value. The lighter down-type squark ( $\tilde{d}_{1,2,3}$ ) and the charged slepton loop contributions to this width are suppressed by the small  $Re(H_1^0)$  component of  $h^0$ . The chargino loops can also contribute to this width, but they can not be enhanced by the large trilinear couplings  $T_{U23,32,33}$ . The  $H^+$  boson loop contribution to this width is strongly suppressed by its large mass  $m_{H^+}$  ( $\simeq m_{A^0}$ ) in our decoupling Higgs scenario with large  $m_{A^0}$  ( $> 1350$  GeV) and large  $\tan\beta$  ( $> 10$ ) (see Table 1). Here note that the deviation of the MSSM width  $\Gamma(h^0 \rightarrow \gamma\gamma)$  from its SM value is not so large since the  $W^+$  boson loop contribution dominates this width.

## 4.2 Scatter plot analysis

We compute the decay widths  $\Gamma(h^0 \rightarrow X\bar{X})$  ( $X = c, b$ ) and  $\Gamma(h^0 \rightarrow bs) \equiv \Gamma(h^0 \rightarrow b\bar{s}) + \Gamma(h^0 \rightarrow \bar{b}s)$  at full 1-loop level in the  $\overline{DR}$  renormalization scheme in the MSSM



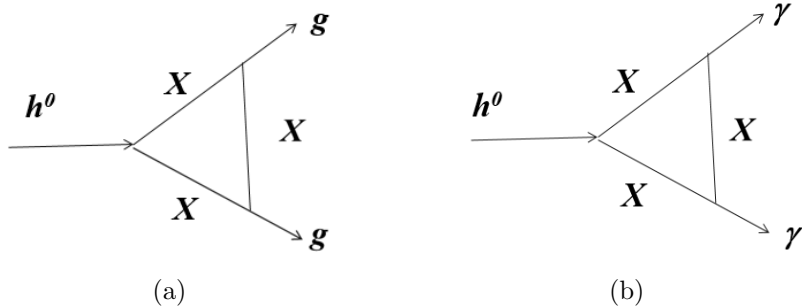


Figure 2: (a) The SM ( $X = \text{top quark}$ ) and MSSM ( $X = \tilde{u}_{1,2,3}$ ) loop contributions to  $\Gamma(h^0 \rightarrow gg)$ , and (b) the SM ( $X = W^+$  boson, top quark) and MSSM ( $X = \tilde{u}_{1,2,3}$ ) loop contributions to  $\Gamma(h^0 \rightarrow \gamma\gamma)$ . The NLO QCD correction diagrams are not shown in these figures. For (a)  $h^0 \rightarrow gg$ , the MSSM ( $\tilde{u}_i$ ) loop diagrams with the contact interactions of  $\tilde{u}_i$ - $\tilde{u}_i$ -gluon-gluon are not shown. For (b)  $h^0 \rightarrow \gamma\gamma$ , the SM ( $W^+$ ) loop diagram with that of W-W- $\gamma$ - $\gamma$  and the MSSM ( $\tilde{u}_i$ ) loop diagrams with those of  $\tilde{u}_i$ - $\tilde{u}_i$ - $\gamma$ - $\gamma$  are not shown.

with general QFV using Fortran codes developed by us [4, 5].<sup>6</sup> We compute the decay widths  $\Gamma(h^0 \rightarrow XX)$  ( $X = g, \gamma$ ) at the NLO QCD level in the  $\overline{DR}$  renormalization scheme in the MSSM with general QFV using Fortran codes developed by us [6].<sup>7</sup> The details of the computation of the decay widths  $\Gamma(h^0 \rightarrow XX)$  ( $X = g, \gamma$ ) at the NLO QCD level in the MSSM with general QFV are explained in Section 3 of [6] (see especially footnote 1 in Section 3 of [6]).

In the following we will show scatter plots in various planes related with these decay widths obtained from the MSSM parameter scan described above (see Table 1), respecting all the relevant constraints (see Appendix A).

<sup>6</sup>The SM widths  $\Gamma(h^0 \rightarrow X\bar{X})_{SM}$  ( $X = c, b$ ) are computed in Refs. [31, 32], but we do not use these SM widths. Instead, we compute the SM widths  $\Gamma(h^0 \rightarrow X\bar{X})_{SM}$  ( $X = c, b$ ) by taking the decoupling SUSY/Higgs limit of the MSSM width  $\Gamma(h^0 \rightarrow X\bar{X})_{MSSM}$ , i. e., the limit of large SUSY mass scale  $M_{SUSY}$ , large  $m_{A^0}$  (pole), large  $\tan\beta$  and no SUSY QFV (no squark generation mixing) in order to calculate the relative deviation of the MSSM width  $\Gamma(h^0 \rightarrow X\bar{X})_{MSSM}$  from the SM width  $\Gamma(h^0 \rightarrow X\bar{X})_{SM}$  at full 1-loop level *consistently*. We have obtained  $\Gamma(h^0 \rightarrow c\bar{c})_{SM} = 0.128\text{MeV}$  and  $\Gamma(h^0 \rightarrow b\bar{b})_{SM} = 2.89\text{MeV}$ .

<sup>7</sup>The SM widths  $\Gamma(h^0 \rightarrow XX)_{SM}$  ( $X = g, \gamma$ ) are computed in Refs. [31, 32], but we do not use these SM widths. Instead, we compute the SM widths  $\Gamma(h^0 \rightarrow XX)_{SM}$  ( $X = g, \gamma$ ) at the NLO QCD level by ourselves in order to calculate the relative deviation of the MSSM width  $\Gamma(h^0 \rightarrow XX)_{MSSM}$  from the SM width  $\Gamma(h^0 \rightarrow XX)_{SM}$  at the NLO QCD level *consistently*. We also compute the SM widths  $\Gamma(h^0 \rightarrow XX)_{SM}$  ( $X = g, \gamma$ ) by taking the decoupling SUSY/Higgs limit of the MSSM width  $\Gamma(h^0 \rightarrow XX)_{MSSM}$  at the NLO QCD level. We have found that the former SM widths agree with the latter SM widths very well. We have obtained  $\Gamma(h^0 \rightarrow gg)_{SM} = 0.262\text{MeV}$  and  $\Gamma(h^0 \rightarrow \gamma\gamma)_{SM} = 0.0111\text{MeV}$ .

### 4.2.1 Definition of relative deviations from SM predictions

We define the relative deviation of the decay width  $\Gamma(X)$  ( $\equiv \Gamma(h^0 \rightarrow X\bar{X})$ ) from the SM width as follows:

$$\text{DEV}(X) \equiv \frac{\Gamma(X)}{\Gamma(X)_{SM}} - 1 \quad (X = c, b, g, \gamma). \quad (5)$$

Here  $\Gamma(X)_{SM}$  is the SM prediction for the decay width  $\Gamma(X)$ .

According to Ref. [21] we define the effective  $h^0XX$  coupling  $g(h^0XX)$  as follows:

$$g(h^0XX)^2 \equiv \frac{\Gamma(X)}{\Gamma(X)_{SM}}. \quad (6)$$

As the SM effective coupling  $g(h^0XX)_{SM} = 1$  by definition, the so-called coupling modifier  $\kappa_X$  ( $\equiv g(h^0XX)/g(h^0XX)_{SM}$ ) is equal to  $g(h^0XX)$ . The relative deviation  $\text{DEV}(X)$  is related with the effective coupling  $g(h^0XX)$  and the coupling modifier  $\kappa_X$  as follows:

$$\text{DEV}(X) = g(h^0XX)^2 - 1 = \kappa_X^2 - 1. \quad (7)$$

We define the relative deviation of the width ratio  $\Gamma(X)/\Gamma(Y)$  from its SM prediction as follows:

$$\text{DEV}(X/Y) \equiv \frac{\Gamma(X)/\Gamma(Y)}{\Gamma(X)_{SM}/\Gamma(Y)_{SM}} - 1. \quad (8)$$

Note that we have the following approximation:

$$\text{DEV}(X/Y) \simeq \text{DEV}(X) - \text{DEV}(Y) \quad (\text{for } |\text{DEV}(Y)| \ll 1). \quad (9)$$

It is important to notice that a significant (substantial) part of the experimental systematic and statistical errors of the measured widths  $\Gamma(X)$  and  $\Gamma(Y)$  cancel out in the width ratio  $\Gamma(X)/\Gamma(Y)$ , which results in a relatively small experimental error of the measured width ratio. The theoretical errors of the MSSM widths  $\Gamma(X)_{MSSM}$  and  $\Gamma(Y)_{MSSM}$  also cancel out significantly in the width ratio  $\Gamma(X)_{MSSM}/\Gamma(Y)_{MSSM}$ , which leads to a relatively small theoretical error of the MSSM width ratio; e.g., the phase-space factor proportional to  $1/m_{h^0}$  cancels out in the MSSM width ratio, where we impose the constraint  $m_{h^0} = 125.09 \pm 3.48$  GeV (see Table 5). Therefore, the experimental measurement errors as well as the MSSM prediction uncertainties tend to cancel out significantly in the width ratios, making the measurement of these width ratios a very sensitive probe of virtual SUSY loop effects in these  $h^0$  decays at future lepton colliders. Moreover, as we expect from Eq. (9), the deviation of the MSSM width ratio from the SM prediction can be significantly enhanced compared with that of a single MSSM width from the SM; e.g., we will see below that  $\text{DEV}(\gamma/g)$  can be as large as about +9% (see Fig. 12(c)). Furthermore, there can be significant correlations between the deviation of the single MSSM width from the SM value and that of the MSSM width ratio from the SM; e.g. there is a very strong correlation between  $\text{DEV}(c)$  and  $\text{DEV}(b/c)$  as shown in Fig. 4(a) below.

## 4.2.2 Scatter plots for fermionic decays

### - Scatter plots for DEVs of fermionic decays

In Fig. 3 we show the scatter plot in the DEV(c)-DEV(b) plane obtained from the MSSM parameter scan. DEV(c) and DEV(b) can be quite large simultaneously since large trilinear couplings  $T_{U23}$ ,  $T_{U32}$  and  $T_{U33}$  can enhance both DEV(c) and DEV(b) as explained above. From Fig. 3(a), indeed we see that DEV(c) and DEV(b) can be quite large simultaneously: DEV(c) can be as large as  $\sim \pm 60\%$  and DEV(b) can be as large as  $\sim \pm 20\%$ . Future lepton colliders together with HL-LHC can observe such large deviations from SM at very high significance (see Appendix B); e.g., from Appendix B we see that the expected absolute  $1\sigma$  error of DEV(c) is sufficiently small  $\Delta\text{DEV}(c) = (3.6\%, 2.4\%, 1.8\%)$  and that of DEV(b) is also sufficiently small  $\Delta\text{DEV}(b) = (1.7\%, 1.1\%, 0.9\%)$  at (ILC250, ILC250+500, ILC250+500+1000) together with HL-LHC, respectively (see Fig. 3(a)). The expected absolute  $1\sigma$  errors of DEV(c) and DEV(b) at the other lepton colliders are similar to those at ILC (see Appendix B).

In Fig. 3(b), we show also the ATLAS and CMS data of DEV(b) at 95% CL obtained from the recent  $\kappa_b$  data [47, 48] shown in Table 5 by using the relation  $\text{DEV}(b) = \kappa_b^2 - 1$ :  $\text{DEV}(b) = -0.21^{+0.44}_{-0.33}$  (95% CL) (ATLAS) and  $\text{DEV}(b) = -0.02^{+0.76}_{-0.52}$  (95% CL) (CMS). Here note that the current LHC data of  $\kappa_c$  (and hence, that of DEV(c) also) has very large uncertainties (errors) [47, 48]. We see that both the SM and the MSSM are consistent with the recent ATLAS and CMS data, and that the errors of the recent ATLAS and CMS data are relatively very large.

In Fig. 4(a), we show the scatter plot in the DEV(b/c)-DEV(c) plane obtained from the MSSM parameter scan described in Section 3. We see that there is a strong correlation between DEV(b/c) and DEV(c), and that DEV(b/c) can be quite large for large  $|\text{DEV}(c)|$ : DEV(b/c) can exceed +100% for  $\text{DEV}(c) \lesssim -0.5$ . This strong correlation stems from the fact that the two DEVs have a common origin of enhancement, i. e., the large trilinear couplings  $T_{U23,32,33}$ . This behavior is consistent with the expectation from the argument above.

In Fig. 4(b), we show the scatter plot in the DEV(b/c)-DEV(b) plane obtained from the MSSM parameter scan. We see that there is an appreciable correlation between DEV(b/c) and DEV(b), which comes also from the fact that the two DEVs have a common origin of enhancement, i. e., the large trilinear couplings  $T_{U23,32,33}$  and  $T_{D23,32,33}$ .

### - Scatter plots for QFV decay $h^0 \rightarrow b s$

As for the explicitly QFV decay  $h^0 \rightarrow b s$ , Refs. [14–18] computed  $B(h^0 \rightarrow b s)$  in the MSSM with general QFV. However, they neglected LR and RL squark flavor (generation) mixings which we have found very important. Moreover, the constraints used in [14–18] are incomplete and/or old (obsolete).

Ref. [19] computed  $B(h^0 \rightarrow b s)$  at full 1-loop level in the MSSM with general QFV including LL, RR, LR, RL squark flavor (generation) mixings respecting relevant constraints as we do here. However, some of the constraints used in [19] (including those from B meson

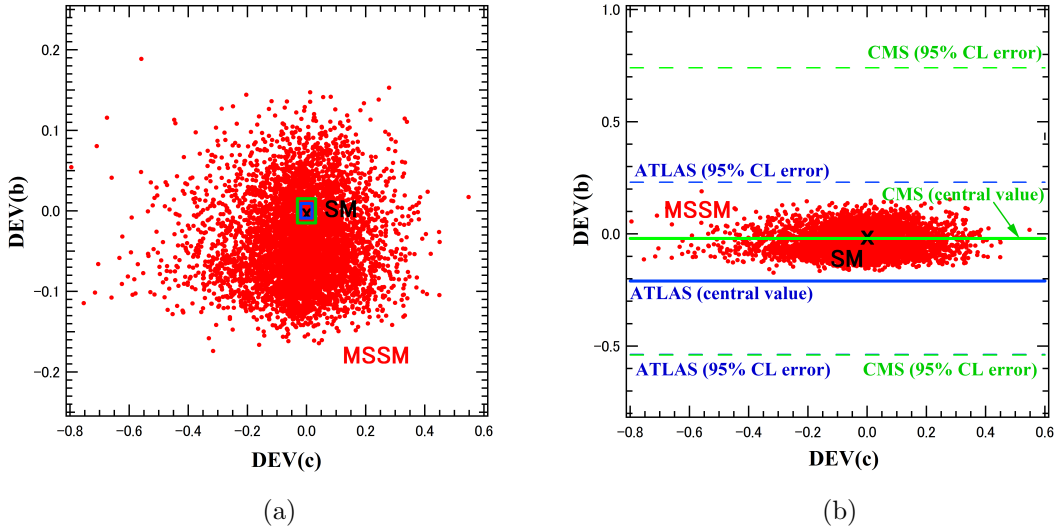


Figure 3: Shown in (a) is the scatter plot in the  $\text{DEV}(c)$ - $\text{DEV}(b)$  plane obtained from the MSSM parameter scan described in Section 3. "X" marks the SM point. The green and blue boxes indicate the expected  $1\sigma$  errors at ILC250 and ILC250+500, respectively (see Table 6). Though in principle the expected  $1\sigma$  error should be shown by an error ellipse, here it is shown by an error box as an approximation since such  $1\sigma$  error ellipse in the  $\kappa_c$ - $\kappa_b$  plane (and hence, in the  $\text{DEV}(c)$ - $\text{DEV}(b)$  plane) is not given in [20, 21]. The expected absolute  $1\sigma$  errors at the other lepton colliders are similar to those at ILC (see Table 6). In (b) we show also the ATLAS and CMS data of  $\text{DEV}(b)$  obtained from the recent  $\kappa_b$  data [47, 48] by using the  $\text{DEV}(b)$ - $\kappa_b$  relation  $\text{DEV}(b) = \kappa_b^2 - 1$ .

data) are already obsolete; e.g., they performed a  $B(h^0 \rightarrow bs)$  contour plot analysis in the squark flavor mixing parameter planes in six benchmark scenarios (S1-S6). All of the benchmark scenarios except S5 are already excluded by the recent gluino mass limit from LHC,  $m_{\tilde{g}} > 2.35$  TeV for  $m_{\tilde{\chi}_1^0} < 1.55$  TeV (see Appendix A).

In the present work, we update these constraints (including the B meson data) and perform a systematic MSSM parameter scan respecting the updated constraints. Furthermore, we take into account also the expected mass limits for the SUSY particles and the heavier MSSM Higgs bosons  $H^0$ ,  $A^0$ ,  $H^\pm$  from the future HL-LHC experiment. We compute  $B(h^0 \rightarrow bs)$  approximately from the full 1-loop level width  $\Gamma(h^0 \rightarrow bs)$  in the MSSM with general QFV by dividing it by the LO total width of the  $h^0$  decay obtained from the public code `SPheno-v3.3.8` [27, 28].

In Fig. 5 we show the scatter plot in the  $B(h^0 \rightarrow bs)$ - $\text{DEV}(b)$  plane obtained from the MSSM parameter scan described in Section 3. We see that  $B(h^0 \rightarrow bs)$  can be as large as  $\sim 0.1\%$  and that  $B(h^0 \rightarrow bs)$  and  $\text{DEV}(b)$  can be sizable simultaneously. This is due to the fact that  $B(h^0 \rightarrow bs)$  and  $\text{DEV}(b)$  have a common origin of enhancement, i. e., large

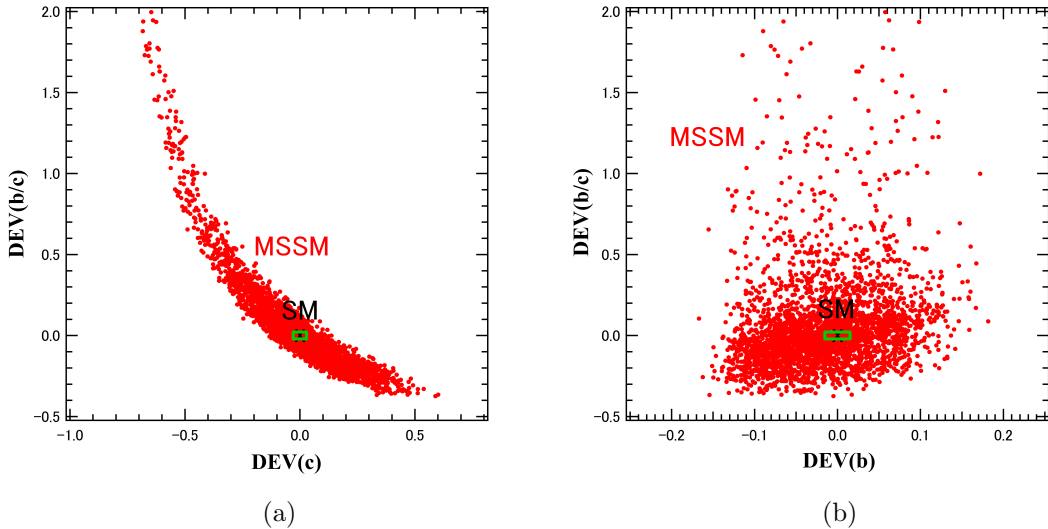


Figure 4: The scatter plot in the (a)  $\text{DEV}(c)$ - $\text{DEV}(b/c)$  and (b)  $\text{DEV}(b)$ - $\text{DEV}(b/c)$  planes obtained from the MSSM parameter scan described in Section 3. "X" marks the SM point. The expected absolute  $1\sigma$  errors at ILC250 shown by the green box are given by  $(\Delta\text{DEV}(c), \Delta\text{DEV}(b), \Delta\text{DEV}(b/c))=(3.6\%, 1.7\%, 3.1\%)$  (see Table 6). Though, in principle, the expected  $1\sigma$  error should be shown by an error ellipse, here it is shown by an error box as an approximation. The expected absolute  $1\sigma$  errors at the other lepton colliders are similar to those at ILC (see Table 6).

trilinear couplings  $T_{U23,32,33}$  and  $T_{D23,32,33}$  (see Fig. 1(b) and Fig. 1(c)).

On the other hand, from our contour plot analysis of the branching ratio  $B(h^0 \rightarrow bs)$  shown below in Fig. 10(c), we find that it can be as large as  $\sim 0.15\%$  respecting all the updated constraints including the expected mass limits for the SUSY particles and the heavier MSSM Higgs bosons from the future HL-LHC experiment. Here we remark that [19] found that  $B(h^0 \rightarrow bs)$  can be as large as  $\sim O(0.1\%)$ , however, respecting already outdated constraints in the MSSM with general QFV. It is very small ( $B(h^0 \rightarrow bs) \lesssim 10^{-7}$ ) in the SM [14,54,55]. The ILC250+500+1000 sensitivity to this branching ratio  $B(h^0 \rightarrow bs)$  could be  $\sim 0.1\%$  at  $4\sigma$  signal significance [56] (see also [57]) (see Appendix C). Hence, such QFV decay  $h^0 \rightarrow bs$  in the MSSM with general QFV can be observed at ILC with very high signal significance.<sup>8</sup> Note that the LHC and HL-LHC sensitivity to this QFV decay branching ratio should not be so good due to huge QCD background [57].

Here we comment on the effect of resummation of the bottom Yukawa coupling for  $\Gamma(h^0 \rightarrow b\bar{b})$  and  $\Gamma(h^0 \rightarrow bs)$  in the MSSM. We have studied the effect of the resummation of the bottom Yukawa coupling for large  $\tan\beta$  [62]. It turns out that in our case with large  $m_{A^0}$  close to the decoupling Higgs limit (see Table 1), the resummation effect (the

<sup>8</sup>The expected upper bound on  $B(h^0 \rightarrow bs)$  at FCC-ee is [60]:  $B(h^0 \rightarrow bs) < 4.5 \cdot 10^{-4}$  (95% CL). The expected upper bound on  $B(h^0 \rightarrow bs)$  at CEPC is [61]:  $B(h^0 \rightarrow bs) < 2.2 \cdot 10^{-4}$  (95% CL).

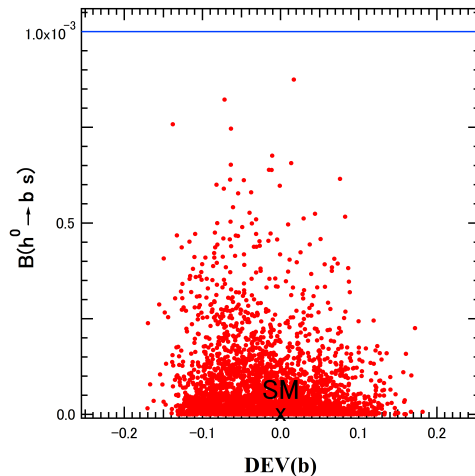


Figure 5: The scatter plot in the  $B(h^0 \rightarrow bs)$ - $\text{DEV}(b)$  plane obtained from the MSSM parameter scan described in Section 3. The blue horizontal line indicates the ILC250+500+1000 sensitivity to  $B(h^0 \rightarrow bs)$  of  $\sim 0.1\%$  at  $4\sigma$  signal significance. "X" marks to the SM point.

so-called  $\Delta_b$  effect) is very small ( $< 0.1\%$ ) [5, 63].

### 4.2.3 Scatter plots for bosonic decays

#### - Scatter plot in $\text{DEV}(\gamma)$ - $\text{DEV}(g)$ plane

In Fig. 6 we show the scatter plot in the  $\text{DEV}(\gamma)$ - $\text{DEV}(g)$  plane obtained from the MSSM parameter scan. We see that there is a strong correlation between  $\text{DEV}(\gamma)$  and  $\text{DEV}(g)$ . This correlation is due to the fact that the lighter up-type squark ( $\tilde{u}_{1,2,3}$ ) loop (stop-scharm mixture loop) contributions dominate the two DEVs. From Fig. 6(a) we see that  $\text{DEV}(\gamma)$  and  $\text{DEV}(g)$  can be sizable simultaneously:  $\text{DEV}(\gamma)$  can be as large as  $\sim \pm 1\%$  and  $\text{DEV}(g)$  can be as large as  $\sim \pm 4\%$ . ILC together with HL-LHC can observe such sizable deviation  $\text{DEV}(g)$  at fairly high significance though they can not observe such moderate deviation  $\text{DEV}(\gamma)$  significantly (see Appendix B): The expected absolute  $1\sigma$  error of  $\text{DEV}(\gamma)$  is  $\Delta\text{DEV}(\gamma) = (2.4\%, 2.2\%, 2.0\%)$  and that of  $\text{DEV}(g)$  is  $\Delta\text{DEV}(g) = (1.8\%, 1.4\%, 1.1\%)$  at (ILC250, ILC250+500, ILC250+500+1000) together with HL-LHC, respectively (see Fig. 6(a)). The expected absolute  $1\sigma$  errors of  $\text{DEV}(\gamma)$  and  $\text{DEV}(g)$  at the other lepton colliders are similar to those at ILC (see Appendix B). It is important to note that  $\text{DEV}(g)$  can be as large as  $\sim -7\%$  as can be seen in the contour plot of Fig. 11(c) in the following, which corresponds to more than  $5\sigma$  deviation from the SM at ILC250+500 and ILC250+500+1000. We would see this fact if we generate much more MSSM parameter points in our parameter scan.

In Fig. 6(b), we show also the ATLAS and CMS data of  $\text{DEV}(\gamma)$  and  $\text{DEV}(g)$  at 95% CL obtained from the recent ATLAS and CMS data of  $\kappa_\gamma$  and  $\kappa_g$  [47, 48] by using the

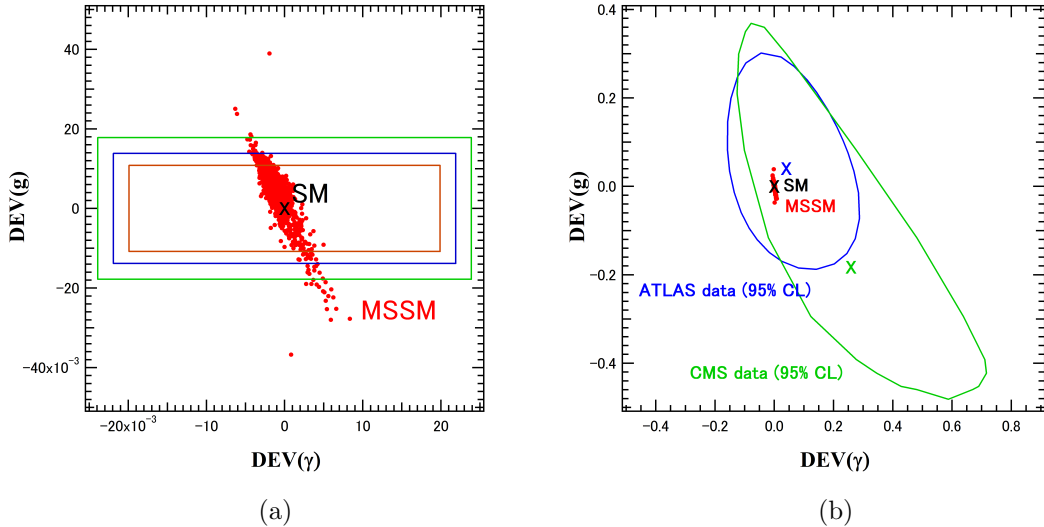


Figure 6: In (a), we show the scatter plot in the  $\text{DEV}(\gamma)$ - $\text{DEV}(g)$  plane obtained from the MSSM parameter scan described in Section 3. "X" marks the SM point. The green, blue and brown boxes indicate the expected  $1\sigma$  errors at ILC250, ILC250+500 and ILC250+500+1000, respectively (see Table 6). Though, in principle, the expected  $1\sigma$  error should be shown by an error ellipse, here it is shown by an error box as an approximation since such  $1\sigma$  error ellipse in the  $\kappa_\gamma$ - $\kappa_g$  plane (and hence, in the  $\text{DEV}(\gamma)$ - $\text{DEV}(g)$  plane) is not given in [20,21]. The expected absolute  $1\sigma$  errors at the other lepton colliders are similar to those at ILC (see Table 6). We have confirmed that all the constraints in Appendix A are satisfied at the MSSM parameter points corresponding to the two isolated points with  $\text{DEV}(g) \sim \pm 4\%$  in (a). In (b), we show also the ATLAS and CMS data of  $\text{DEV}(\gamma)$  and  $\text{DEV}(g)$  at 95% CL obtained from the recent ATLAS and CMS data of  $\kappa_\gamma$  and  $\kappa_g$  [47,48] by using the relation  $\text{DEV}(X) = \kappa_X^2 - 1$ . The black, blue and green "X" marks the SM point, and the central values of the ATLAS and CMS data, respectively.

relation  $\text{DEV}(X) = \kappa_X^2 - 1$ . We see that both the SM and the MSSM are allowed by the recent ATLAS and CMS data and that the errors of the ATLAS and CMS data are too large to distinguish the MSSM from the SM.

### 4.3 Contour plot analysis

#### 4.3.1 Benchmark scenario

In order to see the relevant MSSM parameter dependence of  $\text{DEV}(b)$ ,  $\text{DEV}(c)$ ,  $\text{DEV}(b/c)$ ,  $B(h^0 \rightarrow bs)$ ,  $\text{DEV}(\gamma)$ ,  $\text{DEV}(g)$  and  $\text{DEV}(\gamma/g)$  in more detail, we take a reference scenario P1 where we have sizable  $\text{DEV}(b)$ ,  $\text{DEV}(c)$ ,  $\text{DEV}(b/c)$ ,  $B(h^0 \rightarrow bs)$ ,  $\text{DEV}(\gamma)$ ,  $\text{DEV}(g)$  and  $\text{DEV}(\gamma/g)$  and then variate the relevant MSSM parameters around this point P1. All MSSM input parameters for P1 are shown in Table 2, where one has  $\text{DEV}(c) = -0.11$ ,

$\text{DEV}(b) = -0.15$ ,  $\text{DEV}(b/c) = -0.042$ ,  $B(h^0 \rightarrow bs) = 0.040\%$ ,  $\text{DEV}(\gamma) = 0.011$ ,  $\text{DEV}(g) = -0.045$  and  $\text{DEV}(\gamma/g) = 0.059$ . The scenario P1 satisfies all the present experimental and theoretical constraints shown in Appendix A. The resulting physical masses of the particles are shown in Table 3. The flavor decompositions of the lighter squarks  $\tilde{u}_{1,2,3}$  and  $\tilde{d}_{1,2,3}$  are shown in Table 4. For the calculation of the masses and the mixings of the sparticles and the MSSM Higgs bosons, as well as for the low-energy observables, especially those in the B and K meson sectors (see Table 5), we use the public code **SPheno** v3.3.8 [27, 28]. As for the effective mixing angle  $\alpha$  in the CP even neutral Higgs boson sector, we obtain  $\alpha = -0.0303$  with  $H^0 = \cos \alpha(\sqrt{2}\text{Re}(H_1^0) - v_1) + \sin \alpha(\sqrt{2}\text{Re}(H_2^0) - v_2)$  and  $h^0 = -\sin \alpha(\sqrt{2}\text{Re}(H_1^0) - v_1) + \cos \alpha(\sqrt{2}\text{Re}(H_2^0) - v_2)$ .

We compute the coupling modifier  $\kappa_X$  by using  $\text{DEV}(X) = \kappa_X^2 - 1$  (see Eq. (7)). We obtain  $\kappa_b = 0.922$  ( $\text{DEV}(b) = -0.15$ ),  $\kappa_g = 0.977$  ( $\text{DEV}(g) = -0.045$ ) and  $\kappa_\gamma = 1.005$  ( $\text{DEV}(\gamma) = 0.011$ ) in the scenario P1, which satisfy the LHC data in Table 5. For the other coupling modifiers, and the invisible decay branching ratio  $B_{inv}$  and the undetected decay branching ratio  $B_{und}$ , see Appendix D.

Furthermore, we have confirmed that in all contour plots shown below the red hatched regions (which include always our reference point P1) satisfy all the constraints in Appendix A and also all the expected sparticle mass limits and  $(m_{A^0}, \tan \beta)$  limit from the negative search for the sparticles and the MSSM Higgs bosons  $H^0$ ,  $A^0$ ,  $H^\pm$  in the future HL-LHC experiments [97–103]. In this confirmation, we have used contour plots of all the sparticle masses in the individual parameter plane.

Here, concerning the constraint from the negative searches for the MSSM Higgs bosons at LHC, we remark the following point: In all contour plots,  $m_{A^0}$  is fixed to be  $\simeq 5.3$  TeV and hence  $m_{H^0, A^0, H^\pm} \simeq 5.3$  TeV for which  $H^0$ ,  $A^0$ ,  $H^\pm$  are obviously too heavy to be produced at LHC(13TeV) and HL-LHC(14TeV). Here note that  $m_{H^0} \simeq m_{A^0} \simeq m_{H^\pm}$  in the decoupling Higgs limit in the MSSM. Hence, the entire contour plot planes are allowed by the negative search for the MSSM Higgs bosons  $H^0$ ,  $A^0$ ,  $H^\pm$  at LHC(13TeV) and HL-LHC(14TeV).

### 4.3.2 Contour plots for fermionic decays

In Fig. 7 we show contours of  $\text{DEV}(b)$  around the benchmark point P1 in various parameter planes. Fig. 7(a) shows contours of  $\text{DEV}(b)$  in the  $T_{U23}$ - $T_{U32}$  plane. We see that  $|\text{DEV}(b)|$  increases quickly with the increase of  $|T_{U23}|$  and  $|T_{U32}|$  as expected. We also see that it is large ( $-0.18 \lesssim \text{DEV}(b) \lesssim -0.13$ ) respecting all the constraints in a significant part of this parameter plane. From Fig. 7(b), we see that  $\text{DEV}(b)$  is also sensitive to  $T_{U33}$  and can be as large as  $\sim -0.18$ . As can be seen in Fig. 7(c),  $\text{DEV}(b)$  is fairly sensitive to  $M_{U23}^2$ , especially for large  $|T_{U32}| \gtrsim 3$  TeV, as expected, and is large ( $-0.18 \lesssim \text{DEV}(b) \lesssim -0.15$ ) respecting all the constraints in a significant part of this parameter plane.

As for the contours of  $\text{DEV}(b)$  around P1 in the planes of down-type squark parameters  $T_{D23}$ ,  $T_{D32}$ ,  $T_{D33}$  and  $M_{D23}^2$ , we have found that  $\text{DEV}(b)$  is rather insensitive to these parameters as expected: the weaker dependence of  $\text{DEV}(b)$  on the down-type squark



Table 2: The MSSM parameters for the reference point P1 (in units of GeV or GeV<sup>2</sup> except for  $\tan\beta$ ). All parameters are defined at scale  $Q = 1$  TeV, except  $m_{A^0}(pole)$ . The parameters that are not shown here are taken to be zero.

$\tan\beta$	$M_1$	$M_2$	$M_3$	$\mu$	$m_{A^0}(pole)$														
33	1660	765	4615	870	5325														
$M_{Q22}^2$	$M_{Q33}^2$	$M_{Q23}^2$	$M_{U22}^2$	$M_{U33}^2$	$M_{U23}^2$														
3975 <sup>2</sup>	3160 <sup>2</sup>	920 <sup>2</sup>	3465 <sup>2</sup>	1300 <sup>2</sup>	795 <sup>2</sup>														
$M_{D22}^2$	$M_{D33}^2$	$M_{D23}^2$	$T_{U23}$	$T_{U32}$	$T_{U33}$														
2620 <sup>2</sup>	2425 <sup>2</sup>	-1625 <sup>2</sup>	-2040	-1880	-4945														
$T_{D23}$	$T_{D32}$	$T_{D33}$	$T_{E33}$																
-2360	1670	-2395	-300																
$M_{Q11}^2$	$M_{U11}^2$	$M_{D11}^2$	$M_{L11}^2$	$M_{L22}^2$	$M_{L33}^2$	$M_{E11}^2$	$M_{E22}^2$	$M_{E33}^2$											
4500 <sup>2</sup>	4500 <sup>2</sup>	4500 <sup>2</sup>	1500 <sup>2</sup>	1500 <sup>2</sup>	1500 <sup>2</sup>	1500 <sup>2</sup>	1500 <sup>2</sup>	1500 <sup>2</sup>											

parameters such as  $T_{D23}$  than that on the up-type squark parameters such as  $T_{U23}$  stems from the fact that the  $\tilde{d}_{1,2,3} - \tilde{g}$  loops (Fig. 1(c)) are less important than the  $\tilde{u}_{1,2,3} - \tilde{\chi}_{1,2}^\pm$  loops (Fig. 1(b)) mainly due to the small  $Re(H_1^0)$  component of  $h^0$  in our decoupling Higgs scenario, which suppresses the  $h^0 - \tilde{d}_i - \tilde{d}_j$  couplings.

As shown in Table 6, the expected absolute  $1\sigma$  error of  $DEV(b)$  measured at ILC is given by  $\Delta DEV(b) = (1.7\%, 1.1\%, 0.9\%)$  at (ILC250, ILC250+500, ILC250+500+1000) and similar results are obtained for the future lepton colliders other than ILC. Therefore, such large deviation  $DEV(b)$  ( $\sim -15\%$  to  $-20\%$ ) in the sizable region allowed by all the constraints (including the expected sparticle and MSSM Higgs boson mass limits from HL-LHC) as shown in Fig. 7 can be observed with very high significance at the future lepton colliders such as ILC.

Just to show how the allowed parameter region is affected by the change of the total theoretical error of  $m_{h^0}$ , we have drawn  $m_{h^0}$  bound lines in the contour plots of  $DEVs$  and  $B(h^0 \rightarrow bs)$  in the hypothetical case that the total theoretical error is  $\pm 2$  GeV instead of  $\pm 3$  GeV. As can be seen in Figs. 7 - 8 and Figs. 10 - 12, the allowed parameter region is only a little affected by the change of the total theoretical error.

In Fig. 8 we show contour plots of  $DEV(c)$  around the benchmark point P1 in various parameter planes. Fig. 8(a) shows contours of  $DEV(c)$  in the  $T_{U23}$ - $T_{U32}$  plane. We see that  $DEV(c)$  is sensitive to  $T_{U23}$  and  $T_{U32}$ :  $|DEV(c)|$  quickly increases with the increase of  $T_{U23}$  and  $T_{U32}$  as expected (see Fig. 1(a) and the related argument above). We find

Table 3: Physical masses in GeV of the particles for the scenario of Table 2.

$m_{\tilde{\chi}_1^0}$	$m_{\tilde{\chi}_2^0}$	$m_{\tilde{\chi}_3^0}$	$m_{\tilde{\chi}_4^0}$	$m_{\tilde{\chi}_1^+}$	$m_{\tilde{\chi}_2^+}$
781	882	911	1669	782	914

$m_{h^0}$	$m_{H^0}$	$m_{A^0}$	$m_{H^+}$
124	5325	5325	5359

$m_{\tilde{g}}$	$m_{\tilde{u}_1}$	$m_{\tilde{u}_2}$	$m_{\tilde{u}_3}$	$m_{\tilde{u}_4}$	$m_{\tilde{u}_5}$	$m_{\tilde{u}_6}$
4424	868	3011	3331	3877	4402	4402

$m_{\tilde{d}_1}$	$m_{\tilde{d}_2}$	$m_{\tilde{d}_3}$	$m_{\tilde{d}_4}$	$m_{\tilde{d}_5}$	$m_{\tilde{d}_6}$
1705	2833	3010	3877	4397	4403

$m_{\tilde{\nu}_1}$	$m_{\tilde{\nu}_2}$	$m_{\tilde{\nu}_3}$	$m_{\tilde{l}_1}$	$m_{\tilde{l}_2}$	$m_{\tilde{l}_3}$	$m_{\tilde{l}_4}$	$m_{\tilde{l}_5}$	$m_{\tilde{l}_6}$
1509	1509	1528	1489	1489	1509	1512	1512	1545

Table 4: Flavor decompositions of the mass eigenstates  $\tilde{u}_{1,2,3}$  and  $\tilde{d}_{1,2,3}$  for the scenario of Table 2. Shown are the expansion coefficients of the mass eigenstates in terms of the flavor eigenstates. Imaginary parts of the coefficients are negligibly small.

	$\tilde{u}_L$	$\tilde{c}_L$	$\tilde{t}_L$	$\tilde{u}_R$	$\tilde{c}_R$	$\tilde{t}_R$
$\tilde{u}_1$	0.0001	-0.0190	-0.0959	0	0.0767	-0.9922
$\tilde{u}_2$	-0.0283	-0.0736	0.9740	0	0.1978	-0.0775
$\tilde{u}_3$	0.0088	0.0288	-0.1886	0	0.9771	0.0932
	$\tilde{d}_L$	$\tilde{s}_L$	$\tilde{b}_L$	$\tilde{d}_R$	$\tilde{s}_R$	$\tilde{b}_R$
$\tilde{d}_1$	0	-0.0012	0.0099	0	0.6585	0.7525
$\tilde{d}_2$	0	-0.0058	0.0448	0	-0.7521	0.6575
$\tilde{d}_3$	-0.0018	-0.1183	0.9919	0	0.0274	-0.0373

also that  $\text{DEV}(c)$  is sizable ( $-0.15 \lesssim \text{DEV}(c) \lesssim -0.05$ ) respecting all the constraints in a significant part of this parameter plane. From Fig. 8(b), we see that  $\text{DEV}(c)$  is sensitive also to  $T_{U33}$ , quickly increases with the increase of  $|T_{U33}|$  as expected, and it is large ( $-0.20 \lesssim \text{DEV}(c) \lesssim -0.05$ ) respecting all the constraints in a sizable part of this parameter plane. As can be seen in Fig. 8(c),  $\text{DEV}(c)$  is sensitive to  $T_{U32}$  and  $M_{U23}^2$  increasing with the increase of  $T_{U32}$  and  $M_{U23}^2$  as expected and is quite large ( $-0.25 \lesssim \text{DEV}(c) \lesssim 0.1$ ) respecting all the constraints in a significant part of this parameter plane. Note that  $\text{DEV}(c)$  is especially large for the large product  $T_{U32} \cdot M_{U23}^2 (< 0)$ . This is due to the following reason:

(i) The gluino loop contribution (Fig. 1(a)) to the decay amplitude for  $h^0 \rightarrow c\bar{c}$  can be very large positive or negative for a large value of the product  $T_{U32} \cdot M_{U23}^2$  since the leading gluino loop contribution is proportional to the product  $T_{U32} \cdot M_{U23}^2$  in terms of the mass-insertion (MI) approximation (see Fig. 9) [5].

(ii) Hence, the interference term between the tree diagram and the gluino loop contribution of Fig. 1(a) can be very large (positive or negative) for a large value of the product  $T_{U32} \cdot M_{U23}^2$ , which can lead to even *negative* width  $\Gamma(h^0 \rightarrow c\bar{c})$  at one-loop level. In this case the perturbation theory breaks down.

(iii) Therefore, in principle, the deviation of  $\Gamma(h^0 \rightarrow c\bar{c})$  from the SM value ( $\text{DEV}(c)$ ) can be very large for a large value of the product  $T_{U32} \cdot M_{U23}^2$ .

As for the contours of  $\text{DEV}(c)$  around P1 in the planes of down-type squark parameters  $T_{D23}$ ,  $T_{D32}$ ,  $T_{D33}$  and  $M_{D23}^2$ , we have found that  $\text{DEV}(c)$  is insensitive to these parameters as expected: the main MSSM 1-loop corrections to  $\Gamma(h^0 \rightarrow c\bar{c})$  stem from  $\tilde{u}_{1,2,3}$  -  $\tilde{g}$  loops (see Fig. 1(a)), which do not involve the down-type squark parameters.

As shown in Table 6, the expected absolute  $1\sigma$  error of  $\text{DEV}(c)$  measured at ILC is given by  $\Delta\text{DEV}(c) = (3.6\%, 2.4\%, 1.8\%)$  at (ILC250, ILC250+500, ILC250+500+1000) and similar results are obtained for the future lepton colliders other than ILC. Hence, such large deviation  $\text{DEV}(c)$  ( $\sim +10\%$  to  $-25\%$ ) in the sizable region allowed by all the constraints (including the expected sparticle mass limits from HL-LHC) as shown in Fig. 8 can be observed with very high significance at the future lepton colliders such as ILC.

In Fig. 10 we show contours of  $B(h^0 \rightarrow bs)$  around the benchmark point P1 in various parameter planes. Fig. 10(a) shows contours of  $B(h^0 \rightarrow bs)$  in the  $T_{U23}$ - $T_{U32}$  plane. We see that  $B(h^0 \rightarrow bs)$  is sensitive to both  $T_{U23}$  and  $T_{U32}$ , increases with the increase of  $|T_{U23}|$  and  $|T_{U32}|$ , as expected (see Fig. 1(b)), and can be as large as about 0.00045 in the allowed region. From Fig. 10(b), we see that  $B(h^0 \rightarrow bs)$  is also sensitive to  $T_{U33}$ , increases with the increase of  $|T_{U33}|$ , as expected, and can be as large as about 0.0006 in the allowed region. From Fig. 10(c), we find that  $B(h^0 \rightarrow bs)$  is also sensitive to  $\tan\beta$  as expected and can be as large as about 0.0015 in the allowed region. We also see that it is sizable ( $0.00025 \lesssim B(h^0 \rightarrow bs) \lesssim 0.0015$ ) respecting all the constraints in a significant part of this parameter plane. From Fig. 10(d) we see that  $B(h^0 \rightarrow bs)$  is sensitive to both  $T_{D23}$  and  $T_{D32}$  (being the  $\tilde{s}_R$  -  $\tilde{b}_L$  and  $\tilde{s}_L$  -  $\tilde{b}_R$  mixing parameter, respectively), increases with the increase of  $|T_{D23}|$  and  $|T_{D32}|$  (with  $T_{D23} \cdot T_{D32} < 0$ ), as expected, and can reach 0.001 in the allowed region.

The  $4\sigma$  signal significance sensitivity to  $B(h^0 \rightarrow bs)$  of ILC250+500+1000 is  $B(h^0 \rightarrow bs) = 0.001$  as mentioned above. Hence, such large  $B(h^0 \rightarrow bs)$  ( $\sim 0.001$  to  $0.0015$ ) in the region allowed by all the constraints (including the expected sparticle mass limits from HL-LHC) as shown in Figs. 10 can be observed at ILC with high significance.

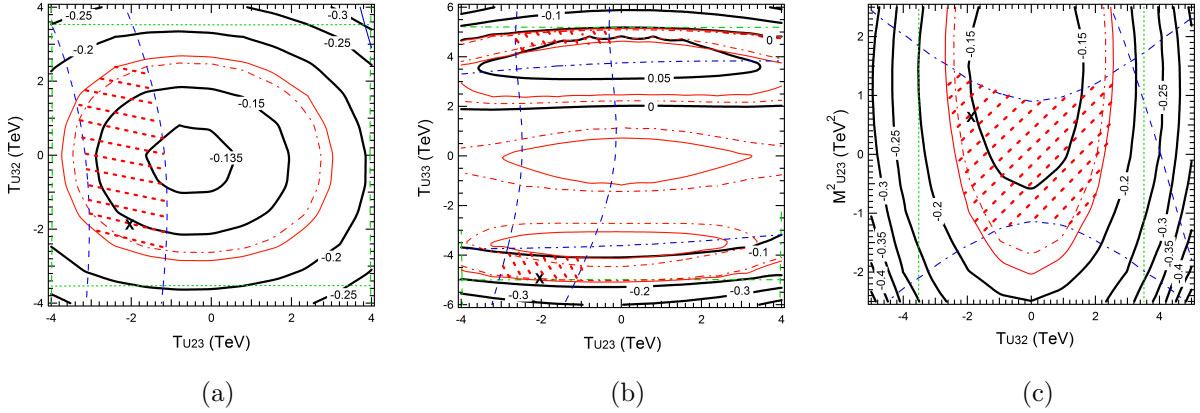


Figure 7: Contour plots of  $\text{DEV}(b)$  around the benchmark point P1 in the parameter planes of (a)  $T_{U23} - T_{U32}$ , (b)  $T_{U23} - T_{U33}$ , and (c)  $T_{U32} - M_{U23}^2$ . The parameters other than the shown ones in each plane are fixed as in Table 2. The "X" marks P1 in the plots. The red hatched region satisfies all the constraints in Appendix A and also all the expected sparticle mass limits and  $(m_{A^0}, \tan \beta)$  limit at 95% CL from negative search for sparticles and the heavier MSSM Higgs bosons  $H^0$ ,  $A^0$ ,  $H^\pm$  in the future HL-LHC experiments [97–103]. The red solid lines, green dashed lines, green dotted lines, green dash-dotted lines, blue solid lines, blue dashed lines, and blue dash-dotted lines show the  $m_{h^0}$  bound, vacuum stability bound for  $T_{U23}$ ,  $T_{U32}$ ,  $T_{U33}$ ,  $B(b \rightarrow s\gamma)$  bound,  $B(B_s \rightarrow \mu^+\mu^-)$  bound, and  $m_{\tilde{u}_1}$  bound, respectively. Just for reference, the red dash-dotted lines show the  $m_{h^0}$  bounds for a hypothetical case that the total theoretical error is  $\pm 2$  GeV instead of  $\pm 3$  GeV; i.e. the contours of  $m_{h^0}$  (GeV) =  $125.09 + (0.48 + 2) = 127.57$  and  $m_{h^0}$  (GeV) =  $125.09 - (0.48 + 2) = 122.61$ . We see that only a small part of the red hatched region is excluded by this hypothetical  $m_{h^0}$  bounds.

### 4.3.3 Contour plots for bosonic decays

In Fig. 11 we show contour plots of  $\text{DEV}(g)$  around the benchmark point P1 in various parameter planes. Fig. 11(a) shows contours of  $\text{DEV}(g)$  in the  $T_{U23}-T_{U32}$  plane. We see that  $\text{DEV}(g)$  is fairly sensitive to  $T_{U23}$  and  $T_{U32}$  as expected (see Fig. 2(a) and the related argument above). It is sizable ( $-0.05 \lesssim \text{DEV}(g) \lesssim -0.044$ ) in the allowed region. From Fig. 11(b), we see that  $\text{DEV}(g)$  is also sensitive to  $T_{U33}$  increasing quickly with the increase of  $|T_{U33}|$  as expected. As can be seen in Fig. 11(c),  $\text{DEV}(g)$  is sensitive to  $M_{U23}^2$  increasing with the increase of  $|M_{U23}^2|$  as expected from decreasing  $m_{\tilde{u}_1}$  for increasing  $|M_{U23}^2|$ , and it is sizable ( $-0.07 \lesssim \text{DEV}(g) \lesssim -0.045$ ) in the allowed region.

As for the contours of  $\text{DEV}(g)$  around P1 in the planes of the down-type squark parameters  $T_{D23}$ ,  $T_{D32}$ ,  $T_{D33}$  and  $M_{D23}^2$ , we have found that  $\text{DEV}(g)$  is insensitive to these parameters as expected.

As shown in Table 6, the expected absolute  $1\sigma$  error of  $\text{DEV}(g)$  measured at ILC is given by  $\Delta\text{DEV}(g) = (1.8\%, 1.4\%, 1.1\%)$  at (ILC250, ILC250+500, ILC250+500+1000),

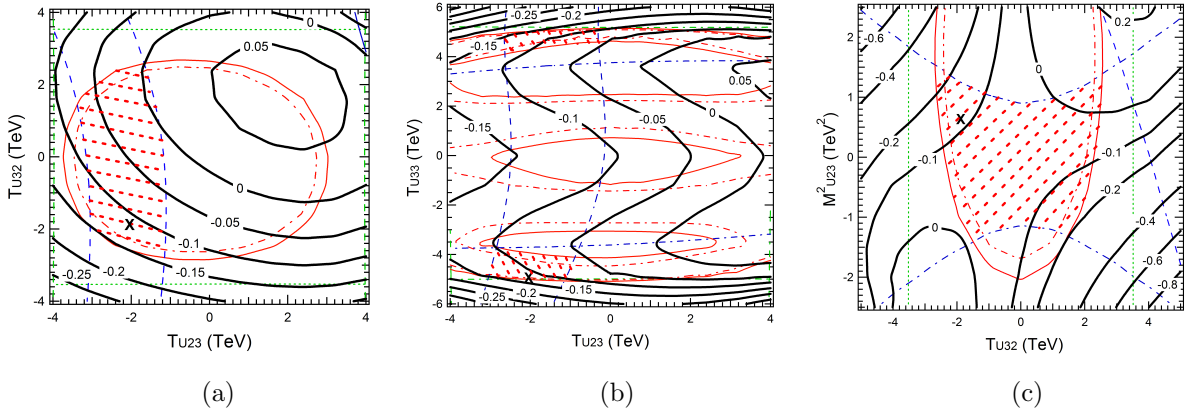


Figure 8: Contour plots of  $\text{DEV}(c)$  around the benchmark point P1 in the parameter planes of (a)  $T_{U23} - T_{U32}$ , (b)  $T_{U23} - T_{U33}$  and (c)  $T_{U32} - M_{U23}^2$ . The parameters other than the shown ones in each plane are fixed as in Table 2. The "X" marks P1 in the plots. The definitions of the red hatched regions and the bound lines are the same as those in Fig. 7.

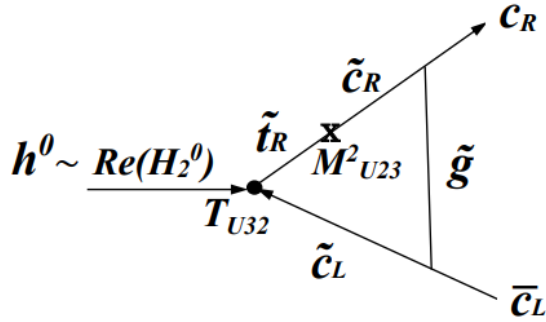


Figure 9: The leading gluino loop contribution to the decay amplitude for  $h^0 \rightarrow c\bar{c}$  in terms of the MI approximation.

and similar results are obtained for the future lepton colliders other than ILC. Hence, such large deviation  $\text{DEV}(g)$  ( $\sim -4\%$  to  $-7\%$ ) in the sizable region allowed by all the constraints (including the expected sparticle mass limits from HL-LHC) as shown in Fig. 11 can be observed with high significance at the future lepton colliders such as ILC.

As for contour plots of  $\text{DEV}(\gamma)$  around the benchmark point P1, we have found that the tendency of them is similar to that of  $\text{DEV}(g)$ , except the overall normalization and sign. This is due to the fact that, as can be seen in Fig. 6(a), for any MSSM parameter point, approximately we have (see [6] also)

$$\text{DEV}(\gamma) \sim -\frac{1}{4}\text{DEV}(g). \quad (10)$$

In Fig. 12, we show contour plots of  $\text{DEV}(\gamma/g)$  around the benchmark point P1 in

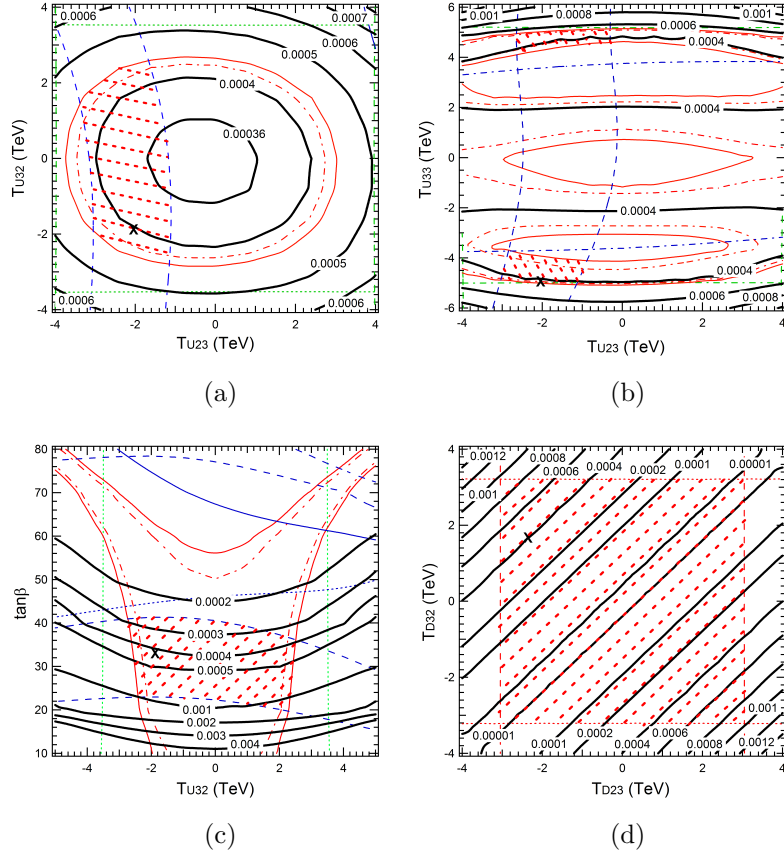


Figure 10: Contour plots of  $B(h^0 \rightarrow bs)$  around the benchmark point P1 in the parameter planes of (a)  $T_{U23} - T_{U32}$ , (b)  $T_{U23} - T_{U33}$ , (c)  $T_{U32} - \tan\beta$ , and (d)  $T_{D23} - T_{D32}$ . The parameters other than the shown ones in each plane are fixed as in Table 2. The "X" marks P1 in the plots. Note that  $4\sigma$  signal significance sensitivity to  $B(h^0 \rightarrow bs)$  of ILC250+500+1000 is  $B(h^0 \rightarrow bs) = 0.001$ . The definitions of the red hatched regions and the bound lines are the same as those in Fig. 7. In addition to these the blue dotted lines, the red dashed lines and red dotted lines show the  $\Delta M_{B_s}$  bound, and the vacuum stability bound for  $T_{D23}$  and  $T_{D32}$ , respectively. In Figs. 10(a)-10(c), we see that only a small part of the red hatched region is excluded by the hypothetical  $m_{h^0}$  bounds mentioned in Fig. 7. The entire region of Fig. 10(d) is allowed by the hypothetical  $m_{h^0}$  bounds.

various parameter planes. Fig. 12(a) shows contours of  $\text{DEV}(\gamma/g)$  in the  $T_{U23}-T_{U32}$  plane. We see that  $\text{DEV}(\gamma/g)$  is fairly sensitive to  $T_{U23}$  and  $T_{U32}$  as expected (see Fig. 2 and the related argument above). It is sizable ( $0.06 \lesssim \text{DEV}(\gamma/g) \lesssim 0.07$ ) in the allowed region. From Fig. 12(b), we see that  $\text{DEV}(\gamma/g)$  is also sensitive to  $T_{U33}$ , quickly increases with increase of  $|T_{U33}|$  as expected. As can be seen in Fig. 12(c),  $\text{DEV}(\gamma/g)$  is also sensitive to  $M_{U23}^2$  increasing with the increase of  $|M_{U23}^2|$  as expected from decreasing  $m_{\tilde{u}_1}$  for increasing  $|M_{U23}^2|$ , and it is large ( $0.06 \lesssim \text{DEV}(\gamma/g) \lesssim 0.09$ ) in the allowed region. As for the contours of  $\text{DEV}(\gamma/g)$  around P1 in the planes of down-type squark parameters  $T_{D23}$ ,

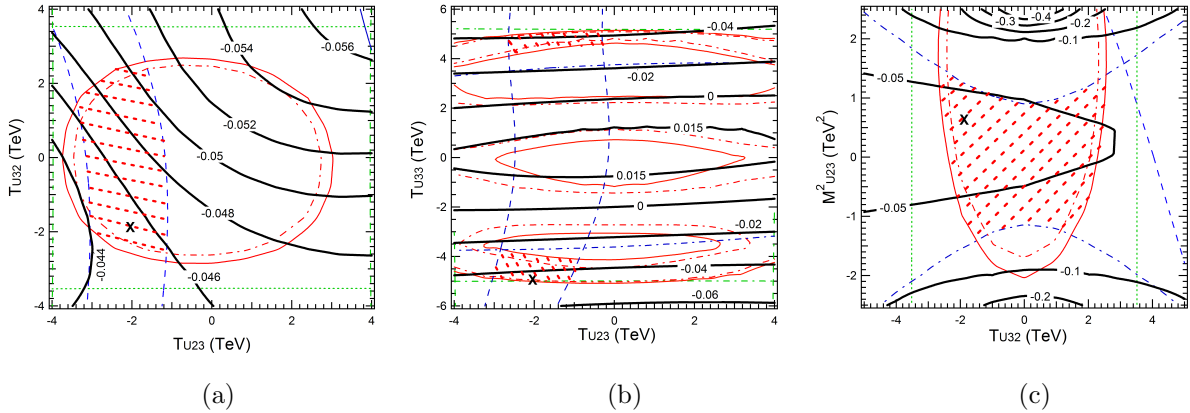


Figure 11: Contour plots of  $\text{DEV}(g)$  around the benchmark point P1 in the parameter planes of (a)  $T_{U23} - T_{U32}$ , (b)  $T_{U23} - T_{U33}$  and (c)  $T_{U32} - M_{U23}^2$ . The parameters other than the shown ones in each plane are fixed as in Table 2. The "X" marks P1 in the plots. The definitions of the red hatched regions and the bound lines are the same as those in Fig. 7.

$T_{D32}$ ,  $T_{D33}$  and  $M_{D23}^2$ , we have found that  $\text{DEV}(\gamma/g)$  is insensitive to these parameters as expected.

As shown in Table 6, the expected absolute  $1\sigma$  error of  $\text{DEV}(\gamma/g)$  measured at ILC is given by  $\Delta\text{DEV}(\gamma/g) = (3.3\%, 2.8\%, 2.3\%)$  at (ILC250, ILC250+500, ILC250+500+1000) and similar results are obtained for the future lepton colliders other than ILC. Therefore, such large deviation  $\text{DEV}(\gamma/g)$  ( $\sim +6\%$  to  $+9\%$ ) in the sizable region allowed by all the constraints (including the expected sparticle mass limits from HL-LHC) as shown in Fig. 12 can be observed with fairly high significance at the future lepton colliders such as ILC.

#### 4.4 Theoretical errors of the MSSM prediction for DEVs

Before closing this section we comment briefly on the theoretical error of the MSSM prediction  $\text{DEV}(X)_{MSSM}$ . We find that, in general, the theoretical error of the MSSM prediction  $\text{DEV}(X)_{MSSM}$  tends to be significantly small compared with the expected experimental error of the  $\text{DEV}(X)$  measured at the future lepton colliders [4, 6]. The theoretical error of the MSSM prediction  $\text{DEV}(X)_{MSSM}$  comes from two sources. One is the parametric uncertainty, and the other is the renormalization scale-dependence uncertainty. The former is due to the errors of the SM input parameters such as  $\alpha_s^{\overline{MS}}(m_Z)$  and the latter is due to unknown higher order corrections. The main reason of this tendency is as follows: the theoretical errors (the parametric errors and the scale-dependence errors) of  $\Gamma(X)_{MSSM}$  and  $\Gamma(X)_{SM}$  significantly cancel out in the ratio  $\Gamma(X)_{MSSM}/\Gamma(X)_{SM}$  in the MSSM prediction  $\text{DEV}(X)_{MSSM} = \Gamma(X)_{MSSM}/\Gamma(X)_{SM} - 1$ , resulting in a significantly small theoretical error of  $\text{DEV}(X)_{MSSM}$ . Here, note that we compute the SM widths  $\Gamma(X)_{SM}$  by taking the decoupling SUSY/Higgs limit of the MSSM width  $\Gamma(X)_{MSSM}$ .

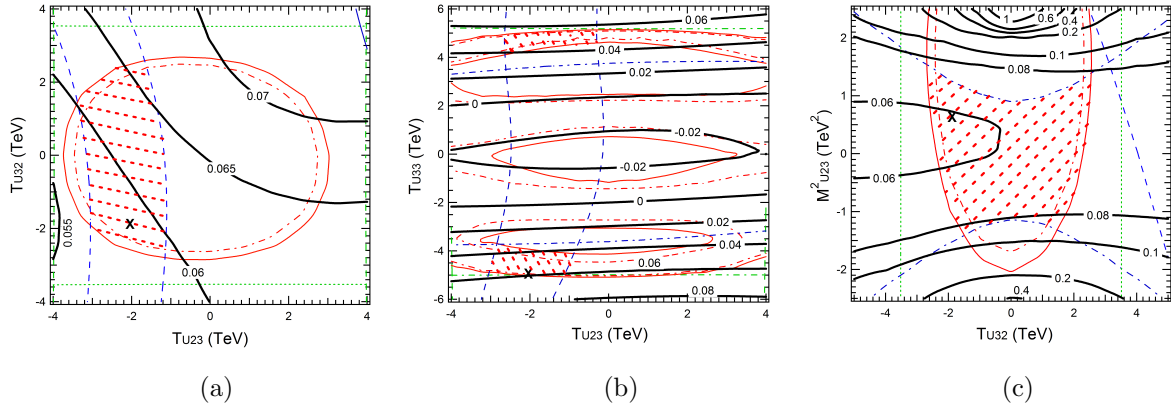


Figure 12: Contour plots of  $\text{DEV}(\gamma/g)$  around the benchmark point P1 in the parameter planes of (a)  $T_{U23} - T_{U32}$ , (b)  $T_{U23} - T_{U33}$  and (c)  $T_{U32} - M_{U23}^2$ . The parameters other than the shown ones in each plane are fixed as in Table 2. The "X" marks P1 in the plots. The definitions of the red hatched regions and the bound lines are the same as those in Fig. 7.

For example, as for the MSSM prediction  $\text{DEV}(g)_{\text{MSSM}}$  at the benchmark point P1, by using the theoretical error estimation method described in [6], we find that the parametric absolute  $1\sigma$  error is 0.073% and the scale-dependence absolute error is 0.080%. Hence, we find the total theoretical absolute  $1\sigma$  error of the MSSM prediction of  $\text{DEV}(g)$  at P1 is 0.153% ( $= 0.073\% + 0.080\%$ ) by adding the parametric absolute  $1\sigma$  error to the scale-dependence absolute error linearly. On the other hand, the expected experimental absolute  $1\sigma$  error of  $\text{DEV}(g)$  is 1.8%, 1.4%, 1.1% at ILC250, ILC250+500, ILC250+500+1000 together with HL-LHC, respectively (see Table 6). Therefore, we find that indeed the theoretical error of the MSSM prediction of  $\text{DEV}(g)$  is significantly small compared with the expected experimental error of  $\text{DEV}(g)$  measured at the future lepton colliders such as ILC.

## 5 Summary and Conclusion

We have studied the decays  $h^0(125) \rightarrow c\bar{c}, b\bar{b}, b\bar{s}, \gamma\gamma, gg$  in the MSSM with general QFV due to squark generation mixings. *In strong contrast to* the usual studies in the MSSM with Minimal Flavor Violation, we have found that the deviations of these MSSM decay widths from the SM values can be quite sizable. *For the first time*, we have performed a systematic MSSM parameter scan for these decay widths respecting all relevant theoretical and experimental constraints. From the parameter scan, we have found the following:

- $\text{DEV}(c)$  and  $\text{DEV}(b)$  can be very large simultaneously:  $\text{DEV}(c)$  can be as large as  $\sim \pm 60\%$ , and  $\text{DEV}(b)$  can be as large as  $\sim \pm 20\%$  (see Fig. 3)
- $\text{DEV}(b/c)$  can exceed  $\sim +100\%$  (see Fig. 4)



- $B(h^0 \rightarrow bs)$  can be as sizable as  $\sim 0.15\%$  exceeding the ILC250+500+1000 sensitivity of  $\sim 0.1\%$  at  $4\sigma$  signal significance (see Fig. 10(c))
- $\text{DEV}(\gamma)$  and  $\text{DEV}(g)$  can be sizable simultaneously:  $\text{DEV}(\gamma)$  can become  $\sim \pm 1\%$ , and  $\text{DEV}(g)$  can be as large as  $\sim +4\%$  and  $\sim -7\%$  (see Fig. 6 and Fig. 11(c))
- $\text{DEV}(\gamma/g)$  can be as large as  $\sim +9\%$  (see Fig. 12(c))
- There are significant correlations among these DEVs and  $B(h^0 \rightarrow bs)$ :
  - There is a very strong correlation between  $\text{DEV}(b/c)$  and  $\text{DEV}(c)$  (see Fig. 4(a))
  - There is a significant correlation between  $B(h^0 \rightarrow bs)$  and  $\text{DEV}(b)$  (see Fig. 5)
  - There is a very strong correlation between  $\text{DEV}(\gamma)$  and  $\text{DEV}(g)$ . This correlation is due to the fact that the  $\tilde{u}_{1,2,3}$ -loop contributions dominate in the two DEVs (see Fig. 6)
- We have pointed out that the experimental measurement uncertainties as well as the MSSM prediction uncertainties tend to cancel out significantly in the width ratios, making the measurement of these width ratios a very sensitive probe of virtual SUSY loop effects in these  $h^0$  decays at future lepton colliders.
- All of these sizable deviations in the  $h^0$  decays are due to (i) large scharm-stop mixing and large scharm/stop involved trilinear couplings  $T_{U23}, T_{U32}, T_{U33}$ , (ii) large sstrange-sbottom mixing and large sstrange/sbottom involved trilinear couplings  $T_{D23}, T_{D32}, T_{D33}$ , and (iii) large bottom Yukawa coupling  $Y_b$  for large  $\tan \beta$  and large top Yukawa coupling  $Y_t$ .

Such sizable deviations from the SM can be observed at high signal significance in future lepton colliders such as ILC, CLIC, CEPC, FCC-ee, and MuC *even after* the failure of SUSY particle discovery at the HL-LHC. In case the deviation pattern shown here is really observed at the lepton colliders, then it would strongly suggest the discovery of QFV SUSY (the MSSM with general QFV).

## Acknowledgments

We would like to thank Werner Porod for helpful discussions, especially for the permanent support concerning SPheno. We also thank Junping Tian and Jorge de Blas for supplying us helpful information on the experiments at the future lepton colliders, especially at ILC. We also thank Sven Heinemeyer for helpful discussions.

## A Theoretical and experimental constraints

The experimental and theoretical constraints taken into account in the present work are discussed in detail in [33]. Here we list the updated constraints from  $K$ - and  $B$ -physics and those on the Higgs boson mass and couplings in Table 5. For the mass of the Higgs boson  $h^0$ , taking the combination of the ATLAS and CMS measurements  $m_{h^0} = 125.09 \pm 0.24$  GeV [43] and adding the theoretical uncertainty of  $\sim \pm 3$  GeV [44] linearly to the experimental uncertainty at  $2\sigma$ , we take  $m_{h^0} = 125.09 \pm 3.48$  GeV.

Here, we remark that the uncertainty of  $\sim \pm 3$  GeV is the intrinsic theoretical error due to unknown higher-order corrections (i.e., the error due to renormalization scheme/scale dependence). It is well known that the parametric uncertainties due to the experimental errors of the SM input parameters (such as  $m_t$ ,  $\alpha_s(m_Z)$ , ...) are also important [45, 46]. The dominant source of the parametric uncertainties is the experimental error of the top quark mass  $m_t$  [46] since the radiative corrected  $m_{h^0}$  is very sensitive to  $m_t$  in the MSSM. Therefore, the total theoretical error given by the sum of the intrinsic theoretical error and the parametric errors should be significantly larger than  $\pm 3$  GeV. Here, we take  $\pm 3$  GeV as the total theoretical error conservatively. It is important to note that the parametric errors, especially that due to experimental error of the top quark mass, remain to be significant even if the intrinsic theoretical error is improved to be very small.

The  $h^0$  couplings that receive SUSY QFV effects significantly are  $g(hbb)$  [5],  $g(hcc)$  [4],  $g(hgg)$  and  $g(h\gamma\gamma)$  [6].<sup>9</sup> The measurement of  $g(hcc)$  is very difficult due to the huge QCD background at LHC; there is no significant experimental data on  $g(hcc)$  at this time. Hence, the relevant  $h^0$  couplings to be compared with the LHC observations are  $g(hbb)$ ,  $g(hgg)$  and  $g(h\gamma\gamma)$ . Therefore, we list the LHC data on  $g(hbb)$  ( $\kappa_b$ ),  $g(hgg)$  ( $\kappa_g$ ) and  $g(h\gamma\gamma)$  ( $\kappa_\gamma$ ) in Table 5.

As the constraints from the decays  $B \rightarrow D^{(*)} \tau \nu$  are unclear due to large theoretical uncertainties [4],<sup>10</sup> we do not take these constraints into account in our paper. As the issues of possible anomalies of  $R(D^{(*)}) = B(B \rightarrow D^{(*)} \tau \nu) / B(B \rightarrow D^{(*)} \ell \nu)$  with  $\ell = e$  or  $\mu$  are not yet settled [49], we do not take the constraints from these ratios into account either. Note that the possible related anomaly of  $R_{K^{(*)}} = B(B \rightarrow K^{(*)} e^+ e^-) / B(B \rightarrow K^{(*)} \mu^+ \mu^-)$  is gone away now [50].

In [26], the QFV decays  $t \rightarrow qh^0$  with  $q = u, c$ , have been studied in the MSSM with general QFV. It is found that these decays cannot be visible at the current and high luminosity LHC runs due to the very small decay branching ratios  $B(t \rightarrow qh^0)$ , giving no significant constraint on the  $\tilde{c} - \tilde{t}$  and  $\tilde{s} - \tilde{b}$  mixings.

In [51], the QFV decay branching ratio  $B(Z^0 \rightarrow bs) \equiv B(Z^0 \rightarrow b\bar{s}) + B(Z^0 \rightarrow \bar{b}s)$  was

---

<sup>9</sup>Precisely speaking, in principle,  $g(htt)$  coupling could also receive SUSY QFV effects significantly. However, predicting the effective coupling  $g(htt)$  at loop levels in the MSSM is very difficult since its theoretical definition in the context of  $t\bar{t}h$  production at LHC is unclear [64].

<sup>10</sup>As pointed out in [65], the theoretical predictions (in the SM and MSSM) on  $B(B \rightarrow D l \nu)$  and  $B(B \rightarrow D^* l \nu)$  ( $l = \tau, \mu, e$ ) have potentially large theoretical uncertainties due to the theoretical assumptions on the hadronic form factors at the  $BDW^+$  and  $BD^*W^+$  vertices (also at the  $BDH^+$  and  $BD^*H^+$  vertices in the MSSM). Hence, the constraints from these decays are unclear.

studied in the MSSM with general QFV. It was shown that the current best experimental upper limit on  $B(Z^0 \rightarrow bs)$  gives no significant constraint on the  $\tilde{s} - \tilde{b}$  and  $\tilde{c} - \tilde{t}$  mixings. <sup>11</sup>

We comment on the recent data on the anomalous magnetic moment of the muon  $a_\mu$  from the Fermilab experiment [66]. The Fermilab data result in  $5.0\sigma$  discrepancy between the experimental data and the SM prediction [67]. <sup>12</sup> In our scenario with heavy sleptons/sneutrinos with masses of about 1.5 TeV, the MSSM loop contributions to  $a_\mu$  are so small that they can not explain the discrepancy between the new data and the SM prediction. Therefore, in the context of our scenario, this discrepancy should be explained by the loop contributions of another new physics coexisting with SUSY.

We also comment on the recent W boson mass data from CDF II [71], which is about  $+7\sigma$  away from the SM prediction. However, the CDF II data disagrees significantly with the world average of the  $m_W$  data from the other experiments [52]. <sup>13</sup> This issue of the  $m_W$  data is not yet settled. Hence, we do not take into account this  $m_W$  constraint on the MSSM parameters in our analysis.

In addition to these, we also require our scenarios to be consistent with the following experimental constraints:

- The LHC limits on sparticle masses (at 95% CL) [76–80]:

We impose conservative limits for safety though actual limits are somewhat weaker than those shown here. In the context of simplified models, gluino masses  $m_{\tilde{g}} \lesssim 2.35$  TeV are excluded for  $m_{\tilde{\chi}_1^0} < 1.55$  TeV. There is no gluino mass limit for  $m_{\tilde{\chi}_1^0} > 1.55$  TeV. The eightfold degenerate first two generation squark masses are excluded below 1.92 TeV for  $m_{\tilde{\chi}_1^0} < 0.9$  TeV. There is no limit on the masses for  $m_{\tilde{\chi}_1^0} > 0.9$  TeV. We impose this squark mass limit on  $m_{\tilde{u}_3}$  and  $m_{\tilde{d}_3}$ . Bottom-squark masses are excluded below 1.26 TeV for  $m_{\tilde{\chi}_1^0} < 0.73$  TeV. There is no bottom-squark mass limit for  $m_{\tilde{\chi}_1^0} > 0.73$  TeV. Here the bottom-squark mass means the lighter sbottom mass  $m_{\tilde{b}_1}$ . We impose this limit on  $m_{\tilde{d}_1}$  since  $\tilde{d}_1 \sim \tilde{b}_R$  (see Table 4). A typical top-squark mass lower limit is  $\sim 1.26$  TeV for  $m_{\tilde{\chi}_1^0} < 0.62$  TeV. There is no top-squark mass limit for  $m_{\tilde{\chi}_1^0} > 0.62$  TeV. Here the top-squark mass means the lighter stop mass  $m_{\tilde{t}_1}$ . We impose this limit on  $m_{\tilde{u}_1}$  since  $\tilde{u}_1 \sim \tilde{t}_R$  (see Table 4). For sleptons/sneutrinos heavier than the lighter chargino  $\tilde{\chi}_1^\pm$  and the second neutralino  $\tilde{\chi}_2^0$ , the mass limits are  $m_{\tilde{\chi}_1^\pm}, m_{\tilde{\chi}_2^0} > 0.74$  TeV for  $m_{\tilde{\chi}_1^0} \lesssim 0.3$  TeV, and there is no  $m_{\tilde{\chi}_1^\pm}, m_{\tilde{\chi}_2^0}$  limits for  $m_{\tilde{\chi}_1^0} > 0.3$  TeV; for sleptons/sneutrinos lighter than  $\tilde{\chi}_1^\pm$  and  $\tilde{\chi}_2^0$ , the mass limits are  $m_{\tilde{\chi}_1^\pm}, m_{\tilde{\chi}_2^0} > 1.15$  TeV for  $m_{\tilde{\chi}_1^0} \lesssim 0.72$  TeV, and there is no  $m_{\tilde{\chi}_1^\pm}$ ,

<sup>11</sup>Note that no experimental upper limit on  $B(Z^0 \rightarrow bs)$  is listed in PDG2022 [52].

<sup>12</sup>On the other hand, Refs. [68–70] point to agreement of the SM prediction with the current experimental data.

<sup>13</sup>We remark the caveats from Refs. [72, 73]: According to the PDG prescription, the new "scale-factored" world average of  $m_W$  data including the CDF II data is  $+3.2\sigma$  off the SM value used by CDF II. We also note that the new improved ATLAS  $m_W$  data [74] is consistent with their old data [75] and the previous world average [52].

Table 5: Constraints on the MSSM parameters from the  $K$ - and  $B$ -meson data relevant mainly for the mixing between the second and the third generations of squarks and from the data on the  $h^0$  mass and couplings  $\kappa_b, \kappa_g, \kappa_\gamma$ . The fourth column shows constraints at 95% CL obtained by combining the experimental error quadratically with the theoretical uncertainty, except for  $B(K_L^0 \rightarrow \pi^0 \nu \bar{\nu})$ ,  $m_{h^0}$  and  $\kappa_{b,g,\gamma}$ .

Observable	Exp. data	Theor. uncertainty	Constr. (95%CL)
$10^3 \times  \epsilon_K $	$2.228 \pm 0.011$ (68% CL) [25]	$\pm 0.28$ (68% CL) [34]	$2.228 \pm 0.549$
$10^{15} \times \Delta M_K$ [GeV]	$3.484 \pm 0.006$ (68% CL) [25]	$\pm 1.2$ (68% CL) [34]	$3.484 \pm 2.352$
$10^9 \times B(K_L^0 \rightarrow \pi^0 \nu \bar{\nu})$	$< 3.0$ (90% CL) [25]	$\pm 0.002$ (68% CL) [25]	$< 3.0$ (90% CL)
$10^{10} \times B(K^+ \rightarrow \pi^+ \nu \bar{\nu})$	$1.7 \pm 1.1$ (68% CL) [25]	$\pm 0.04$ (68% CL) [25]	$1.7^{+2.16}_{-1.70}$
$\Delta M_{B_s}$ [ps $^{-1}$ ]	$17.757 \pm 0.021$ (68% CL) [25, 35]	$\pm 2.7$ (68% CL) [36]	$17.757 \pm 5.29$
$10^4 \times B(b \rightarrow s \gamma)$	$3.32 \pm 0.15$ (68% CL) [25, 35]	$\pm 0.23$ (68% CL) [37]	$3.32 \pm 0.54$
$10^6 \times B(b \rightarrow s l^+ l^-)$ ( $l = e$ or $\mu$ )	$1.60^{+0.48}_{-0.45}$ (68% CL) [38]	$\pm 0.11$ (68% CL) [39]	$1.60^{+0.97}_{-0.91}$
$10^9 \times B(B_s \rightarrow \mu^+ \mu^-)$	$2.69^{+0.37}_{-0.35}$ (68%CL) [40]	$\pm 0.23$ (68% CL) [41]	$2.69^{+0.85}_{-0.82}$
$10^4 \times B(B^+ \rightarrow \tau^+ \nu)$	$1.06 \pm 0.19$ (68%CL) [35]	$\pm 0.29$ (68% CL) [42]	$1.06 \pm 0.69$
$m_{h^0}$ [GeV]	$125.09 \pm 0.24$ (68% CL) [43]	$\pm 3$ [44]	$125.09 \pm 3.48$
$\kappa_b$	$0.89^{+0.22}_{-0.21}$ (95% CL) [47]		$0.89^{+0.22}_{-0.21}$ (ATLAS)
	$0.99^{+0.33}_{-0.31}$ (95% CL) [48]		$0.99^{+0.33}_{-0.31}$ (CMS)
$\kappa_g$	$0.95^{+0.14}_{-0.13}$ (95% CL) [47]		$0.95^{+0.14}_{-0.13}$ (ATLAS)
	$0.92 \pm 0.16$ (95% CL) [48]		$0.92 \pm 0.16$ (CMS)
$\kappa_\gamma$	$1.01 \pm 0.12$ (95% CL) [47]		$1.01 \pm 0.12$ (ATLAS)
	$1.10 \pm 0.16$ (95% CL) [48]		$1.10 \pm 0.16$ (CMS)

$m_{\tilde{\chi}_2^0}$  limits for  $m_{\tilde{\chi}_1^0} > 0.72$  TeV. For mass degenerate selectrons  $\tilde{e}_{L,R}$  and smuons  $\tilde{\mu}_{L,R}$ , masses below 0.7 TeV are excluded for  $m_{\tilde{\chi}_1^0} < 0.41$  TeV. For mass degenerate staus  $\tilde{\tau}_L$  and  $\tilde{\tau}_R$ , masses below 0.39 TeV are excluded for  $m_{\tilde{\chi}_1^0} < 0.14$  TeV. There is no sneutrino  $\tilde{\nu}$  mass limit from LHC yet. Sneutrino masses below 94 GeV are excluded by LEP200 experiment [25].

- The constraint on  $(m_{A^0, H^+}, \tan \beta)$  (at 95% CL) from the negative searches for the MSSM Higgs bosons  $H^0$ ,  $A^0$  and  $H^+$  at LHC [81–91], where  $H^0$  is the heavier  $CP$ -even neutral Higgs boson and  $H^+$  is the charged Higgs boson:

The  $(m_{A^0, H^+}, \tan \beta)$  limit from the negative search for the heavier MSSM Higgs bosons  $H^0$ ,  $A^0$  and  $H^+$  at LHC depends on the MSSM scenarios (such as hMSSM scenario,  $M_h^{125}$  scenario, ...). However, from [81–91], we find that in general the  $(m_{A^0, H^+}, \tan \beta)$  limits of ATLAS/CMS are rather insensitive to the choice of the MSSM scenarios. Here, note that  $m_{H^0} \simeq m_{A^0} \simeq m_{H^+}$  in the decoupling Higgs scenarios as ours. From ATLAS/CMS data [81–91], especially [89], we find that the  $(m_{A^0}, \tan \beta)$  limit from the negative search for the decay  $H^0/A^0 \rightarrow \tau^+ \tau^-$  (as shown in Fig. 2(c) of [81]) is most important for  $\tan \beta > 10$ . The  $(m_{A^0}, \tan \beta)$  limit (at 95% CL) shown in Fig.2(c) of [81] is the strongest for  $\tan \beta > 10$  among those

obtained in [81–91]. Therefore, we take and respect this strongest ( $m_{A^0}, \tan \beta$ ) limit in our parameter scan analysis for  $\tan \beta > 10$ .

- The experimental limit on SUSY contributions on the electroweak  $\rho$  parameter [92]:  $\Delta\rho (\text{SUSY}) < 0.0012$ .

Furthermore, we impose the following theoretical constraints from the vacuum stability conditions for the trilinear coupling matrices [93]:

$$|T_{U\alpha\alpha}|^2 < 3 Y_{U\alpha}^2 (M_{Q\alpha\alpha}^2 + M_{U\alpha\alpha}^2 + m_2^2), \quad (11)$$

$$|T_{D\alpha\alpha}|^2 < 3 Y_{D\alpha}^2 (M_{Q\alpha\alpha}^2 + M_{D\alpha\alpha}^2 + m_1^2), \quad (12)$$

$$|T_{U\alpha\beta}|^2 < Y_{U\gamma}^2 (M_{Q\beta\beta}^2 + M_{U\alpha\alpha}^2 + m_2^2), \quad (13)$$

$$|T_{D\alpha\beta}|^2 < Y_{D\gamma}^2 (M_{Q\beta\beta}^2 + M_{D\alpha\alpha}^2 + m_1^2), \quad (14)$$

where  $\alpha, \beta = 1, 2, 3$ ,  $\alpha \neq \beta$ ;  $\gamma = \text{Max}(\alpha, \beta)$ , and  $m_1^2 = (m_{H^+}^2 + m_Z^2 \sin^2 \theta_W) \sin^2 \beta - \frac{1}{2}m_Z^2$ ,  $m_2^2 = (m_{H^+}^2 + m_Z^2 \sin^2 \theta_W) \cos^2 \beta - \frac{1}{2}m_Z^2$ . The Yukawa couplings of the up-type and down-type quarks are  $Y_{U\alpha} = \sqrt{2}m_{u_\alpha}/v_2 = \frac{g}{\sqrt{2}} \frac{m_{u_\alpha}}{m_W \sin \beta}$  ( $u_\alpha = u, c, t$ ) and  $Y_{D\alpha} = \sqrt{2}m_{d_\alpha}/v_1 = \frac{g}{\sqrt{2}} \frac{m_{d_\alpha}}{m_W \cos \beta}$  ( $d_\alpha = d, s, b$ ), with  $m_{u_\alpha}$  and  $m_{d_\alpha}$  being the running quark masses at the scale  $Q = 1$  TeV and  $g$  being the SU(2) gauge coupling. All soft SUSY-breaking parameters are given at  $Q = 1$  TeV. As SM parameters we take  $m_Z = 91.2$  GeV and the on-shell top-quark mass  $m_t = 172.9$  GeV [25].

## B Expected experimental errors of the deviations DEVs and the effective Higgs couplings at future lepton colliders

Here we summarize expected experimental *absolute*  $1\sigma$  errors of the deviations  $\text{DEV}(X)$  and  $\text{DEV}(X/Y)$  measured at future lepton colliders.

According to Eq. (7), the expected *absolute*  $1\sigma$  error of the relative deviation  $\text{DEV}(X)$  denoted by  $\Delta\text{DEV}(X)$  is related with the expected *relative*  $1\sigma$  error of the effective coupling  $g(h^0 X X)$  denoted by  $\delta g(h^0 X X)$  as follows:

$$\Delta\text{DEV}(X) \simeq 2\delta g(h^0 X X). \quad (15)$$

In Table 6, we show the expected *absolute*  $1\sigma$  errors of the measured deviations  $\text{DEV}(X)$  and  $\text{DEV}(X/Y)$  denoted by  $\Delta\text{DEV}(X)$  and  $\Delta\text{DEV}(X/Y)$  at future lepton colliders. The errors  $\Delta\text{DEV}(X)$  are obtained by using Eq.(15) and the expected *relative*  $1\sigma$  error of the effective coupling  $\delta g(h^0 X X)$  given in Table 29 of Ref. [21].<sup>14</sup> The errors  $\Delta\text{DEV}(X/Y)$  are obtained according to Ref. [53].

<sup>14</sup>The expected *relative*  $1\sigma$  errors of the effective couplings  $\delta g(h^0 X X)$  given in Table 7 of Ref. [20] are similar to those given in Table 29 of Ref. [21].

Table 6: The expected *absolute*  $1\sigma$  error of the deviations  $\text{DEV}(X)$  and  $\text{DEV}(X/Y)$  (denoted by  $\Delta\text{DEV}(X)$  and  $\Delta\text{DEV}(X/Y)$ ) measured at future lepton colliders: ILC-I = ILC250 + Giga-Z, ILC-II = ILC250+500 + Giga-Z, ILC-III = ILC250+500+1000 + Giga-Z; CLIC-I = CLIC380, CLIC-II = CLIC380+1500, CLIC-III = CLIC380+1500+3000; FCC-ee I = FCC-ee240 + Z/WW, FCC-ee II = FCC-ee240+365 + Z/WW; CEPC-I = CEPC240 + Z/WW, CEPC-II = CEPC240+360 + Z/WW; MuC-I = MuC3TeV, MuC-II = MuC10TeV, MuC-III = MuC10TeV+125GeV. As for ILC, the results without Giga-Z run are almost identical to those with Giga-Z one. The Z/WW denote Z-pole and WW threshold runs. All results except for MuC-I and MuC-II are those from the free- $\Gamma_H$  fit and the results for MuC-I and MuC-II are those from the constrained- $\Gamma_H$  fit, where  $\Gamma_H$  is the total width of the Higgs boson  $h^0$ . The details of run scenarios of the lepton colliders are explained in Ref. [21]. The HL-LHC and LEP/SLD measurements are combined with all lepton collider run scenarios.

	ILC-I	ILC-II	ILC-III	CLIC-I	CLIC-II	CLIC-III
$\Delta\text{DEV}(b)$	1.7%	1.1%	0.9%	2.2%	1.2%	1.1%
$\Delta\text{DEV}(c)$	3.6%	2.4%	1.8%	8.6%	3.8%	3.0%
$\Delta\text{DEV}(\gamma)$	2.4%	2.2%	2.0%	2.6%	2.4%	2.2%
$\Delta\text{DEV}(g)$	1.8%	1.4%	1.1%	2.2%	1.6%	1.4%
$\Delta\text{DEV}(b/c)$	3.1%	2.1%	1.3%	8.2%	3.5%	2.5%
$\Delta\text{DEV}(\gamma/g)$	3.3%	2.8%	2.3%	3.4%	3.1%	2.6%

	FCC-ee I	FCC-ee II	CEPC-I	CEPC-II	MuC-I	MuC-II	MuC-III
$\Delta\text{DEV}(b)$	1.3%	1.2%	0.86%	0.84%	1.8%	0.92%	1.1%
$\Delta\text{DEV}(c)$	2.8%	2.6%	2.4%	2.2%	12.4%	3.8%	3.6%
$\Delta\text{DEV}(\gamma)$	2.4%	2.2%	1.8%	1.8%	2.4%	1.4%	1.5%
$\Delta\text{DEV}(g)$	1.5%	1.4%	0.9%	0.88%	1.7%	0.92%	1.0%
$\Delta\text{DEV}(b/c)$	2.2%	2.1%	2.0%	1.9%	11.9%	3.5%	3.4%
$\Delta\text{DEV}(\gamma/g)$	3.0%	2.9%	2.1%	2.0%	3.2%	1.6%	1.6%

## C ILC sensitivity to the branching ratio $B(h^0 \rightarrow b s)$

The setup conditions for this ILC sensitivity are as follows [56]:

- The signal is the QFV decay  $h^0 \rightarrow b\bar{q}$  and  $h^0 \rightarrow \bar{b}q$  with the light quark  $q = d/s$ . The dominant background is the QFC decay  $h^0 \rightarrow b\bar{b}$ , where either  $b$ -jet or  $\bar{b}$ -jet is misidentified as a light quark-jet (a q-jet). We consider the case  $B(h^0 \rightarrow bq) \equiv B(h^0 \rightarrow b\bar{q}) + B(h^0 \rightarrow \bar{b}q) = 0.1\%$  and take  $B(h^0 \rightarrow b\bar{b}) = 58\%$ .
- As for the efficiencies, the followings are assumed:  
The optimal b-tagging efficiency for a b-jet,  $\epsilon_{b/b}$  is  $\sim 94\%$ .  
The q-tagging efficiency for a q-jet,  $\epsilon_{q/q}$  is  $\sim 90\%$ .

The q-tagging efficiency for a b-jet,  $\epsilon_{q/b}$  is  $\sim 6\%$ .

The b-tagging efficiency for a q-jet,  $\epsilon_{b/q}$  is  $\sim 10\%$ .

The efficiency of other selection cuts,  $\epsilon_{other}$  is assumed to be around 70%, such as that from Higgs mass cut, Z mass cut, angular cuts, etc., which would be needed to suppress background events other than  $h^0 \rightarrow b\bar{b}$ . This 70% efficiency would be common for the signal  $h^0 \rightarrow bq$  and the dominant background  $h^0 \rightarrow b\bar{b}$ .

- Regarding the amount of accumulated data at ILC, the specifications of the H-20 scenario [58] (see also [21, 59]) are adopted basically;

- ILC250 stage;

The total number of  $h^0$  production events  $N_{tot}^{h^0}$  is assumed to be  $\sim 0.5 \cdot 10^6$ , for which the expected significance of the signal  $h^0 \rightarrow bq$ ,  $\sigma_{sig}$  is  $\sim 2\sigma$  in case  $B(h^0 \rightarrow bq) = 0.1\%$ :

$$\sigma_{sig} = N_{sig} / \sqrt{N_{sig} + N_{bg}} \sim 2, \text{ where}$$

$$N_{sig} = N_{tot}^{h^0} \cdot B(h^0 \rightarrow bq) \cdot \epsilon_{b/b} \cdot \epsilon_{q/q} \cdot \epsilon_{other} \sim 300 \text{ and}$$

$$N_{bg} = N_{tot}^{h^0} \cdot B(h^0 \rightarrow b\bar{b}) \cdot 2 \cdot \epsilon_{b/b} \cdot \epsilon_{q/b} \cdot \epsilon_{other} \sim 23000.$$

Alternatively, one can say that the expected upper bound on the branching ratio of the QFV decay,  $h^0 \rightarrow bd/s$ , at 95% CL, is 0.1%:  $B(h^0 \rightarrow bd/s) < 0.1\%$  (95% CL) at ILC250.

- ILC250+500 stage;

The total number of  $h^0$  production events  $N_{tot}^{h^0}$  is increased from  $\sim 0.5 \cdot 10^6$  to  $\sim 1.1 \cdot 10^6$ , for which the expected significance of the signal  $h^0 \rightarrow bq$ ,  $\sigma_{sig}$  is  $\sim 3\sigma$  in case  $B(h^0 \rightarrow bq) = 0.1\%$ .

- ILC250+500+1000 stage;

The total number of  $h^0$  production events  $N_{tot}^{h^0}$  is further increased from  $\sim 1.1 \cdot 10^6$  to  $\sim 2.3 \cdot 10^6$ , for which the expected significance of the signal  $h^0 \rightarrow bq$ ,  $\sigma_{sig}$  is  $\sim 4\sigma$  in case  $B(h^0 \rightarrow bq) = 0.1\%$ .

## D Coupling modifiers $\kappa_X$ , $B_{inv}$ and $B_{und}$

Here we show that the leading-order (LO) coupling modifiers  $\kappa_X$  ( $X = W, Z, t, \tau, \mu, Z\gamma$ ),  $B_{inv}$  and  $B_{und}$  at the benchmark scenario P1 satisfy the corresponding LHC data [47, 48]. In Table 7 we show the LO coupling modifiers  $\kappa_X$  ( $X = W, Z, t, \tau, \mu, Z\gamma$ ),  $B_{inv}$  and  $B_{und}$  at P1 and the corresponding ATLAS/CMS data at 95% CL [47, 48].

Table 7: In this Table we show the LO coupling modifiers  $\kappa_X$  ( $X = W, Z, t, \tau, \mu, Z\gamma$ ),  $B_{inv}$  and  $B_{und}$  in the benchmark scenario P1 and the corresponding LHC data at 95% CL [47, 48].

X	$\kappa_X$ at P1	$\kappa_X$ (95% CL) (ATLAS)	$\kappa_X$ (95% CL) (CMS)
W	0.9999999986	$1.054^{+0.117}_{-0.116}$	$1.02 \pm 0.16$
Z	0.9999999986	$0.993 \pm 0.111$	$1.04 \pm 0.14$
t	0.9999983786	$0.944^{+0.218}_{-0.214}$	$1.01^{+0.22}_{-0.20}$
$\tau$	1.0017641128	$0.929^{+0.143}_{-0.137}$	$0.92 \pm 0.16$
$\mu$	1.0017641128	$1.063^{+0.482}_{-0.595}$	$1.12^{+0.41}_{-0.43}$
$Z\gamma$	0.98351169	$1.377^{+0.607}_{-0.720}$	$1.65^{+0.67}_{-0.73}$
$B_X$	$B_X$ at P1	$B_X$ upper bound (95% CL) (ATLAS)	$B_X$ upper bound (95% CL) (CMS)
$B_{inv}$	0.00283	$B_{inv} < 0.13$	$B_{inv} < 0.17$
$B_{und}$	0	$B_{und} < 0.12$	$B_{und} < 0.16$

We compute the LO  $\kappa_X$  ( $X = W, Z, t, \tau, \mu$ ) using the LO formulas given in [94, 95], in which we input  $\alpha$  and  $\beta$  values at P1:  $\alpha = -0.03034721$  and  $\beta = \tan^{-1}(33) = 1.54050257$ ; e.g.,  $\kappa_W = \kappa_Z = \sin(\beta - \alpha) = \sin(1.54050257 - (-0.03034721)) = 0.99999999857$ . We compute the LO  $\kappa_{Z\gamma}$  at P1 using our own Fortran code [96].<sup>15</sup> We compute the LO  $B_{inv}$  and  $B_{und}$  at P1 using the public code SPheno v3.3.8 [27, 28].<sup>16</sup> From Table 7, we find that the LO coupling modifiers  $\kappa_X$  ( $X = W, Z, t, \tau, \mu, Z\gamma$ ),  $B_{inv}$  and  $B_{und}$  at P1 satisfy the corresponding LHC data at 95% CL [47, 48].

Similarly, we have confirmed that the LO coupling modifiers  $\kappa_X$  ( $X = W, Z, t, \tau, \mu, Z\gamma$ ),  $B_{inv}$  and  $B_{und}$  at all the survival points in our MSSM parameter scan satisfy the corresponding LHC data at 95% CL [47, 48].

<sup>15</sup>We compute the LO MSSM width  $\Gamma(h^0 \rightarrow Z\gamma)_{MSSM}$  at the full 1-loop level at P1 in the MSSM with general QFV and the LO SM width  $\Gamma(h^0 \rightarrow Z\gamma)_{SM}$  at the full 1-loop level in the SM using our own Fortran code [96]. We obtain the LO  $\kappa_{Z\gamma} = 0.98351169$  using  $\kappa_{Z\gamma}^2 = \Gamma(h^0 \rightarrow Z\gamma)_{MSSM} / \Gamma(h^0 \rightarrow Z\gamma)_{SM}$ .

<sup>16</sup>We compute  $B_{inv}$  and  $B_{und}$  at P1 using SPheno v3.3.8 as follows:  $B_{inv} = B(h^0 \rightarrow Z\nu\bar{\nu})B(Z \rightarrow \nu\bar{\nu}) = 0.01413 \cdot 0.20 = 0.00283$ .  $B_{und} = B(h^0 \rightarrow \text{undetected New Physics particles}) = B(h^0 \rightarrow \text{sparticles}) = 0$  as the LSP neutralino mass  $m_{\tilde{\chi}_1^0} = 781\text{GeV}$  at P1.



## References

- [1] G. Aad et al. [ATLAS Collaboration], Phys. Lett. B 716 (2012) 1 [arXiv:1207.7214 [hep-ex]].
- [2] S. Chatrchyan et al. [CMS Collaboration], Phys. Lett. B 716 (2012) 30 [arXiv:1207.7235 [hep-ex]].
- [3] T. Barklow, K. Fujii, S. Jung, R. Karl, J. List, T. Ogawa, M. E. Peskin, and J. Tian, Phys. Rev. D 97 (2018) 053003 [arXiv:1708.08912 [hep-ph]]; see also references therein.
- [4] A. Bartl, H. Eberl, E. Ginina, K. Hidaka and W. Majerotto, Phys. Rev. D 91 (2015) 015007 [arXiv:1411.2840 [hep-ph]].
- [5] H. Eberl, E. Ginina, A. Bartl, K. Hidaka and W. Majerotto, JHEP 06 (2016) 143 [arXiv:1604.02366 [hep-ph]].
- [6] H. Eberl, K. Hidaka and E. Ginina, Int. J. Mod. Phys. A34 (2019) 1950120 [arXiv:1812.08010 [hep-ph]].
- [7] M. Cahill-Rowley, J. Hewett, A. Ismail and T. Rizzo, Phys. Rev. D 90 (2014) 095017 [arXiv:1407.7021 [hep-ph]].
- [8] M. Endo, T. Moroi, and M. Nojiri, JHEP 04 (2015) 176 [arXiv:1502.03959 [hep-ph]].
- [9] A. Arbey et al., Phys. Rev. D106 (2022) 055002 [arXiv:2201.00070 [hep-ph]].
- [10] J. Dickinson et al., "A Grand Scan of the pMSSM Parameter Space for Snowmass 2021", arXiv:2207.05103 [hep-ph].
- [11] T. Bose et al., "Report of the Topical Group on Physics Beyond the Standard Model at Energy Frontier for Snowmass 2021", arXiv:2209.13128; see also references therein.
- [12] M. Narain et al., "The Future of US Particle Physics - The Snowmass 2021 Energy Frontier Report", arXiv:2211.11084; see also references therein.
- [13] A. Brignole, Nucl. Phys. B898 (2015) 644 [arXiv:1504.03273 [hep-ph]].
- [14] S. Bejar, F. Dilme, J. Guasch and J. Sola, JHEP 08 (2004) 018 [arXiv:hep-ph/0402188].
- [15] A. Curiel, M. Herrero and D. Temes, Phys. Rev. D 67 (2003) 075008 [arXiv:hep-ph/0210335].
- [16] D. Demir, Phys. Lett. B 571 (2003) 193 [arXiv:hep-ph/0303249].
- [17] A. Curiel, M. Herrero, W. Hollik, F. Merz and S. Peñaranda, Phys. Rev. D 69 (2004) 075009 [arXiv:hep-ph/0312135].

- [18] G. Barenboim, C. Bosch, J. Lee, M. López-Ibañez and O. Vives, Phys. Rev. D 92 (2015) 095017 [arXiv:1507.08304 [hep-ph]].
- [19] M.E. Gómez, S. Heinemeyer and M. Rehman, Phys. Rev. D 93 (2016) 095021 [arXiv:1511.04342[hep-ph]].
- [20] Jorge de Blas et al., JHEP 01 (2020) 139 [arXiv:1905.03764 [hep-ph]].
- [21] Jorge de Blas et al., "Global SMEFT Fits at Future Colliders", arXiv:2206.08326 [hep-ph].
- [22] M. Cepeda et al., CERN Yellow Rep. Monogr. 7 (2019) 221 [arXiv:1902.00134 [hep-ph]].
- [23] B. C. Allanach *et al.*, Comput. Phys. Commun. **180** (2009) 8 [arXiv:0801.0045 [hep-ph]].
- [24] F. Gabbiani, E. Gabrielli, A. Masiero and L. Silvestrini, Nucl. Phys. B 477 (1996) 321 [arXiv:hep-ph/9604387].
- [25] P.A. Zyla et al. (Particle Data Group), Prog. Theor. Exp. Phys. 2020, 083C01 (2020).
- [26] A. Dedes et al., JHEP 11 (2014) 137 [arXiv:1409.6546 [hep-ph]].
- [27] W. Porod, Comput. Phys. Commun. **153** (2003) 275 [arXiv:hep-ph/0301101].
- [28] W. Porod and F. Staub, Comput. Phys. Commun. **183** (2012) 2458 [arXiv:1104.1573 [hep-ph]].
- [29] For details, see SPheno home page: <https://spheno.hepforge.org/>.
- [30] D. M. Pierce et al., Nucl. Phys. B 491 (1997) 3.
- [31] D. de Florian et al. (LHC Higgs Cross Section Working Group), CERN Yellow Rep. Monogr. 2, 1 (2017) [arXiv:1610.07922 [hep-ph]].
- [32] L. G. Almeida, S. J. Lee, S. Pokorski and J. D. Wells, Phys. Rev. D 89 (2014) 033006 [arXiv:1311.6721 [hep-ph]].
- [33] H. Eberl, E. Ginina, K. Hidaka, Eur. Phys. J C 77 (2017) 189 [arXiv:1702.00348 [hep-ph]].
- [34] J. Brod and M. Gorbahn, Phys. Rev. Lett. 108 (2012) 121801 [arXiv:1108.2036 [hep-ph]].
- [35] Y. Amhis et al. (Heavy Flavor Averaging Group (HFLAV)), Eur. Phys. J. C 81 (2021) 226 [arXiv:1909.12524[hep-ex]].

- [36] T. Jubb, M. Kirk, A. Lenz, and G. Tetlalmatzi-Xolocotzi, Nucl. Phys. B915 (2017) 431 [arXiv:1603.07770 [hep-ph]]; M. Artuso, G. Borissov, and A. Lenz, Rev. Mod. Phys. 88 (2016) 045002 [arXiv:1511.09466 [hep-ph]].
- [37] M. Misiak et al., Phys. Rev. Lett. 114 (2015) 221801 [arXiv:1503.01789[hep-ph]].
- [38] J. P. Lees *et al.* [BABAR Collaboration], Phys. Rev. Lett. 112 (2014) 211802 [arXiv:1312.5364 [hep-ex]].
- [39] T. Huber, T. Hurth and E. Lunghi, Nucl. Phys. B 802 (2008) 40 [arXiv:0712.3009 [hep-ph]].
- [40] Y. Amhis, Talk at the 40th International Conference on High Energy Physics, virtual conference 2020, Prague, Czech Republic, PoS ICHEP2020 (2021) 3 [link to the talk: [https://cds.cern.ch/record/2727203/files/ICHEP\\_Yasmine.pdf](https://cds.cern.ch/record/2727203/files/ICHEP_Yasmine.pdf)].
- [41] C. Bobeth *et al.*, Phys. Rev. Lett. 112 (2014) 101801 [arXiv:1311.0903 [hep-ph]].
- [42] J. M. Roney, Proceedings of the 26th International Symposium on Lepton Photon Interactions at High Energies, San Francisco, USA, 2013, Int. J. Mod. Phys. A 29 No.22 (2014) 1430048 [DOI: <https://doi.org/10.1142/S0217751X14300488>].
- [43] ATLAS and CMS collaborations, Phys. Rev. Lett. 114 (2015) 191803 [arXiv:1503.07589 [hep-ex]].
- [44] S. Borowka, T. Hahn, S. Heinemeyer, G. Heinrich and W. Hollik, Eur. Phys. J. C75 (2015) 424 [arXiv:1505.03133 [hep-ph]].
- [45] B. C. Allanach, A. Djouadi, J. L. Kneur, W. Porod, and P. Slavich, JHEP 09 (2004) 044 [hep-ph/0406166].
- [46] T. Hahn, S. Heinemeyer, W. Hollik, H. Rzehak, and G. Weiglein, Phys. Rev. Lett. 112 (2014) 141801 [arXiv:1312.4937 [hep-ph]].
- [47] G. Aad et al. [ATLAS Collaboration], Nature 607 (2022) 52, Nature 612 (2022) E24 (erratum) [arXiv:2207.00092 [hep-ex]].
- [48] A. Tumasyan et al. [CMS Collaboration], Nature 607 (2022) 60 [arXiv:2207.00043 [hep-ex]]; A. M. Sirunyan et al. [CMS Collaboration], JHEP 07 (2021) 027 [arXiv:2103.06956 [hep-ex]].
- [49] C. Lazzeroni, Plenary talk at The European Physical Society Conference on High Energy Physics (EPS-HEP2023), Hamburg, 2023 [link to the talk: [https://indico.desy.de/event/34916/contributions/142205/attachments/83911/111164/EPS\\_Lazzeroni\\_final.pdf](https://indico.desy.de/event/34916/contributions/142205/attachments/83911/111164/EPS_Lazzeroni_final.pdf)].
- [50] LHCb Collaboration, Phys. Rev. Lett. 131 (2023) 051803 [arXiv:2212.09152 [hep-ex]].

- [51] D. Atwood, S. Bar-Shalom, G. Eilam, and A. Soni, Phys. Rev. D **66** (2002) 093005 [arXiv:hep-ph/0203200].
- [52] R. L. Workman et al. (Particle Data Group), "Review of Particle Physics", Prog. Theor. Exp. Phys. **2022** (2022) 083C01 and 2023 update.
- [53] Private communication with Jorge de Blas who computed the expected *relative*  $1\sigma$  errors of the measured width ratios  $\Gamma(X)/\Gamma(Y)$  denoted by  $\delta[\Gamma(X)/\Gamma(Y)]$  at future lepton colliders by using the same program code as that used in Ref. [21], where  $\Gamma(X) \equiv \Gamma(h^0 \rightarrow X\bar{X})$ . The expected experimental absolute  $1\sigma$  errors  $\Delta\text{DEV}(X/Y)$  at future lepton colliders are obtained by using the following relation:  $\Delta\text{DEV}(X/Y) \simeq \delta[\Gamma(X)/\Gamma(Y)]$ .
- [54] L. G. Benitez-Guzman et al., J. Phys. G: Nucl. Part. Phys. **42** (2015) 085002 [arXiv:1506.02718 [hep-ph]].
- [55] J. F. Kamenik et al., Phys. Rev. D **109** (2024) L011301 [arXiv:2306.17520 [hep-ph]].
- [56] Junping Tian (private communication).
- [57] D. Barducci and A.J. Helmboldt, JHEP **12** (2017) 105 [arXiv:1710.06657[hep-ph]].
- [58] T. Barklow et al., arXiv:1506.07830.
- [59] I. Adachi et al. (ILC International Development Team Collaboration), "The International Linear Collider: Report to Snowmass 2021", arXiv:2203.07622 [physics.acc-ph].
- [60] M. Selvaggi, Talk at FCC Physics Performance Meeting, 18 Mar 2024, <https://indico.cern.ch/event/1392261/>.
- [61] H. Liang, Y. Zhu, Y. Wang, Y. Che, C. Zhou, H. Qu and M. Ruan, Phys. Rev. Lett. **132** (2024) 221802 [arXiv:2310.03440 [hep-ex]]; M. Ruan, Plenary Talk at Higgs2023 Conference, 2023, Beijing [link to the talk: <https://indico.ihep.ac.cn/event/18025/contributions/133704/attachments/74198/90943/Physics%20of%20Higgs%20factory%20-%20v2.pdf>].
- [62] M. Carena et al., Nucl. Phys. B **577** (2000) 88 [arXiv:hep-ph/9912516]; J. Guasch et al., Phys. Rev. D **68** (2003) 115001 [arXiv:hep-ph/0305101].
- [63] E. Ginina, A. Bartl, H. Eberl, K. Hidaka and W. Majerotto, Proceedings of EPS-HEP2015 Conference, Vienna, 2015, PoS(EPS-HEP2015) (2015) 146 [arXiv:1510.03714 [hep-ph]].
- [64] P. Wu et al., Phys. Lett. B **618** (2005) 209 [arXiv:hep-ph/0505086]; S. Dittmaier et al., Phys. Rev. D **90** (2014) 035010 [arXiv:1406.5307 [hep-ph]].
- [65] U. Nierste, S. Trine and S. Westhoff, Phys. Rev. D **78** (2008) 015006 [arXiv:0801.4938 [hep-ph]]; see also references therein.

- [66] D. P. Aguillard et al. (The Muon  $g-2$  Collaboration), Phys. Rev. Lett. 131 (2023) 161802 [arXiv:2308.06230 [hep-ex]].
- [67] T. Aoyama et al., Phys. Rep. 887 (2020) 1.
- [68] S. Borsanyi et al., Nature 593 (2021) 51 [arXiv:2002.12347[hep-lat]].
- [69] G. Venanzoni, Plenary talk at The European Physical Society Conference on High Energy Physics (EPS-HEP2023), Hamburg, 2023, Proc. of Sci. EPS-HEP2023 (2024) 037, <https://pos.sissa.it/449/037/>.
- [70] F.V. Ignatov et al. (CMD-3 Collaboration), Phys. Rev. D 109 (2024) 112002 [arXiv:2302.08834 [hep-ex]].
- [71] T. Aaltonen et al. (CDF Collaboration), Science 376 (2022) 170.
- [72] G. Wilson, Talk at ECFA Higgs Factory seminars: Precision physics in the  $e^+e^- \rightarrow W^+W^-$  region, June 10 2022, <https://indico.cern.ch/event/1163667/>.
- [73] S. Heinemeyer, Talk at IDT-WG3-Phys Open Meeting on  $m_W$ , 12 May 2022, <https://agenda.linearcollider.org/event/9357/>.
- [74] ATLAS Collaboration, ATLAS Note ATLAS-CONF-2023-004, <https://cds.cern.ch/record/2853290>; M. Schott, Talk at 57th Recontres de Moriond - ELECTROWEAK INTERACTIONS AND UNIFIED THEORIES, La Thuile (2023).
- [75] ATLAS Collaboration, Eur. Phys. J. C 78 (2018) 110 [arXiv:1701.07240 [hep-ex]].
- [76] F. Moortgat, Proc. Sci., LeptonPhoton2019 (2019) [link to the talk: [https://indico.cern.ch/event/688643/contributions/3410366/attachments/1891440/3120151/LeptonPhoton\\_SUSY\\_Filip.pdf](https://indico.cern.ch/event/688643/contributions/3410366/attachments/1891440/3120151/LeptonPhoton_SUSY_Filip.pdf)].
- [77] C. Botta, Proc. of Sci. ICHEP2020 (2021) 6 [link to the talk: [https://indico.cern.ch/event/868940/contributions/3905701/attachments/2084745/3502248/ICHEP2020\\_SUSYOverview\\_CBotta.pdf](https://indico.cern.ch/event/868940/contributions/3905701/attachments/2084745/3502248/ICHEP2020_SUSYOverview_CBotta.pdf)]; S. Alderweireldt, Proc. of Sci. ICHEP2020 (2021) 224 [link to the talk: [https://indico.cern.ch/event/868940/contributions/3815895/attachments/2083268/3499407/ATLAS\\_EWKSUSY\\_SAlderweireldt.pdf](https://indico.cern.ch/event/868940/contributions/3815895/attachments/2083268/3499407/ATLAS_EWKSUSY_SAlderweireldt.pdf)].
- [78] ATLAS Collaboration, ATLAS PUB Note, "SUSY May 2020 Summary Plot Update", ATL-PHYS-PUB-2020-013; See also the following Web Page: "Summary plots from the ATLAS Supersymmetry physics group", <https://atlas.web.cern.ch/Atlas/GROUPS/PHYSICS/CombinedSummaryPlots/SUSY/>.
- [79] See the following Web Page: "Run 2 Summary plots – 13 TeV", [https://twiki.cern.ch/twiki/bin/view/CMSPublic/PhysicsResultsSUS#Run\\_2\\_Summary\\_plots\\_13\\_TeV](https://twiki.cern.ch/twiki/bin/view/CMSPublic/PhysicsResultsSUS#Run_2_Summary_plots_13_TeV).

- [80] ATLAS Collaboration, JHEP 02 (2021) 143 [arXiv:2010.14293 [hep-ex]].
- [81] ATLAS Collaboration, Phys. Rev. Lett. 125 (2020) 051801 [arXiv:2002.12223 [hep-ex]].
- [82] CMS Collaboration, JHEP 09 (2018) 007 [arXiv:1803.06553 [hep-ex]].
- [83] ATLAS Collaboration, JHEP 11 (2018) 085 [arXiv:1808.03599 [hep-ex]].
- [84] ATLAS Collaboration, JHEP 06 (2021) 145 [arXiv:2102.10076 [hep-ex]].
- [85] ATLAS Collaboration, JHEP 09 (2018) 139 [arXiv:1807.07915 [hep-ex]].
- [86] CMS Collaboration, JHEP 01 (2020) 096 [arXiv:1908.09206 [hep-ex]].
- [87] CMS Collaboration, JHEP 07 (2019) 142 [arXiv:1903.04560 [hep-ex]].
- [88] ATLAS Collaboration, JHEP 11 (2024) 097 [arXiv:2402.05742 [hep-ex]].
- [89] ATLAS Note, ATL-PHYS-PUB-2024-008, "Summary Plots for Beyond SM Higgs boson searches at ATLAS" (See Fig.1(a)).
- [90] ATLAS Collaboration, Phys. Rev. D111 (2025) 072006 [arXiv:2412.17584 [hep-ex]].
- [91] CMS Collaboration, JHEP 07 (2023) 073 [arXiv:2208.02717 [hep-ex]].
- [92] G. Altarelli, R. Barbieri and F. Caravaglios, Int. J. Mod. Phys. A **13** (1998) 1031 [arXiv:hep-ph/9712368].
- [93] J. A. Casas and S. Dimopoulos, Phys. Lett. B **387** (1996) 107 [arXiv:hep-ph/9606237].
- [94] A. Djouadi, Phys. Rept. 459 (2008) 1 [arXiv:hep-ph/0503173].
- [95] A. Arbey, M. Battaglia, A. Djouadi, F. Mahmoudi, M. Muhlleitner and M. Spira, Phys. Rev. D106 (2022) 055002 [arXiv:2201.00070 [hep-ph]].
- [96] H. Eberl, K. Hidaka and E. Ginina, in preparation for publication.
- [97] X. Cid Vidal et al., "Report from Working Group 3: Beyond the Standard Model physics at the HL-LHC and HE-LHC", CERN Yellow Rep: Monogr. 7 (2019) 585-865 [arXiv:1812.07831 [hep-ph]].
- [98] T. Bose et al., "Report of the Topical Group on Physics Beyond the Standard Model at Energy Frontier for Snowmass 2021", arXiv:2209.13128 [hep-ph].
- [99] ATLAS Collaboration, ATLAS Notes ATL-PHYS-PUB-2012-001, ATL-PHYS-PUB-2013-002, ATL-PHYS-PUB-2014-010, and ATL-PHYS-PUB-2018-048.

- [100] C. M. Berggren, Talk at The European Physical Society Conference on High Energy Physics (EPS-HEP2023) (Hamburg, Germany, 2023) [link to the talk: <https://indico.desy.de/event/34916/contributions/147692/attachments/83876/111001/berggren-eps-hep-susy-aug23.pdf>].
- [101] H. Gilmer, Talk at the 40th International Conference on High Energy Physics, virtual conference (ICHEP2020) (Prague, Czech Republic, 2020), Proc. Sci. ICHEP2020 (2021) 247 [link to the talk: [https://indico.cern.ch/event/868940/contributions/3815948/attachments/2081333/3495936/ICHEP\\_2020-Gilmer.pdf](https://indico.cern.ch/event/868940/contributions/3815948/attachments/2081333/3495936/ICHEP_2020-Gilmer.pdf)].
- [102] M. Narain et al., "The Future of US Particle Physics - The Snowmass 2021 Energy Frontier Report", arXiv:2211.11084 [hep-ex].
- [103] H. Bahl, P. Bechtle, S. Heinemeyer, S. Liebler, T. Stefaniak and G. Weiglein, Eur. Phys. J. C 80 (2020) 916 [arXiv:2005.14536 [hep-ph]].